Likelihood Matching for Diffusion Models

Lei Qian
Center for Data Science
Peking University
leiqian@stu.pku.edu.cn

Wu Su
Center for Data Science
Peking University
ekko_suwu@stu.pku.edu.cn

Yanqi Huang
Guanghua School of Management
Peking University
1900013209@pku.edu.cn

Song Xi Chen [*]
Department of Statistics and Data Science
Tsinghua University
sxchen@tsinghua.edu.cn

Abstract

We propose a Likelihood Matching approach for training diffusion models by first establishing an equivalence between the likelihood of the target data distribution and a likelihood along the sample path of the reverse diffusion. To efficiently compute the reverse sample likelihood, a quasi-likelihood is considered to approximate each reverse transition density by a Gaussian distribution with matched conditional mean and covariance, respectively. The score and Hessian functions for the diffusion generation are estimated by maximizing the quasi-likelihood, ensuring a consistent matching of both the first two transitional moments between every two time points. A stochastic sampler is introduced to facilitate computation that leverages both the estimated score and Hessian information. We establish consistency of the quasi-maximum likelihood estimation, and provide non-asymptotic convergence guarantees for the proposed sampler, quantifying the rates of the approximation errors due to the score and Hessian estimation, dimensionality, and the number of diffusion steps. Empirical and simulation evaluations demonstrate the effectiveness of the proposed Likelihood Matching and validate the theoretical results.

1 Introduction

Generative models and methods facilitate powerful learning of data distributions by generating controlled sequences of synthetic data, and stand as a cornerstone of modern machine learning, driving progress in areas like image synthesis, protein design, and data augmentation (Goodfellow et al., 2014; Sohl-Dickstein et al., 2015; Kobyzev et al., 2020; Watson et al., 2023; Dhariwal & Nichol, 2021; Yang et al., 2023; Chen et al., 2024). The mainstream diffusion methods like the denoising diffusion probabilistic models (DDPMs) (Ho et al., 2020) and the denoising diffusion implicit models (DDIMs) (Song et al., 2021a) have demonstrated state-of-the-art performance in generating high-fidelity samples, particularly in image synthesis (Betker et al., 2023; Esser et al., 2024). Among the leading methods, the score-based generative models (SGMs) (Sohl-Dickstein et al., 2015; Ho et al., 2020; Song et al., 2021c) have achieved remarkable success, producing synthetic samples across various domains. The models typically operate by progressively adding noise to data (forward process) and then learning to reverse this process (reverse process), often guided by estimating the score function (gradient of the log-likelihood) of the perturbed data distributions.

The standard training objective for SGMs is based on score matching (Hyvärinen & Dayan, 2005; Vincent, 2011; Song et al., 2021c), which minimizes the discrepancy between a parameterized score function and the underlying score functions at different noise levels of the diffusion process. While being highly effective empirically, the score matching method provides only an indirect connection to the likelihood of the original data distribution q_0 as an upper bound rather than the likelihood itself. Maximizing the data likelihood directly is the approach for parameter estimation in Statistics, underpinned by attractive properties of the Maximum Likelihood Estimation (MLE),

---

[*]Corresponding author

$$\|\nabla \log q_t(X_t \mid X_0) - s_t(X_t; \phi)\|^2 \qquad\qquad -\sum_{k=1}^{N}\left\{\log|\Sigma_{t_{k-1}|t_k}(X_{t_k}; \phi)| + \left\|\Sigma_{t_{k-1}|t_k}^{-\frac{1}{2}}(X_{t_k}; \phi)\,(X_{t_k} - \mu_{t_{k-1}|t_k}(X_{t_k}; \phi))\right\|^2\right\}$$

$X_0 \longleftarrow \qquad\qquad\qquad\qquad X_T \qquad\qquad X_0 \longleftarrow \qquad\qquad\qquad\qquad X_T$

Reverse SDE (noise → data) $\qquad\qquad$ Reverse SDE (noise → data)

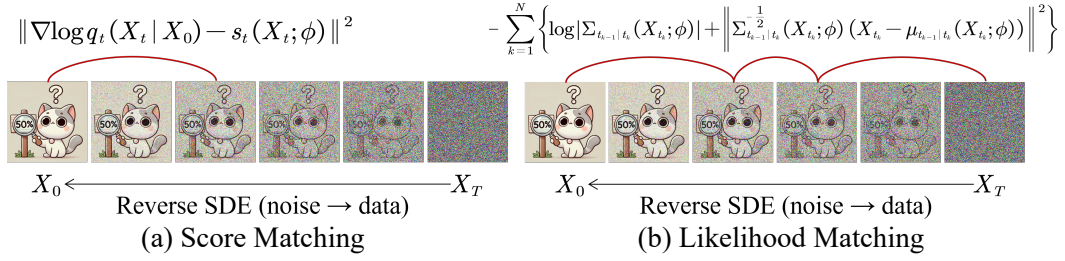(a) Score Matching $\qquad\qquad\qquad\qquad$ (b) Likelihood Matching

Figure 1: Illustration of Score Matching (a) versus Likelihood Matching (b) methods. The proposed Likelihood Matching captures a richer set of transition densities while incorporating both score matching and covariance matching, whereas Score Matching exclusively focuses on a single transition density and utilizes only first-order moment information.

which often yields the most accurate estimators with desirable asymptotic properties like consistency and efficiency.

This paper explores a direct maximum likelihood framework for training diffusion models. We leverage a fundamental property that the path likelihood of the reverse diffusion process is intrinsically equivalent to the likelihood of the original data distribution $q_0(\theta)$ (up to constants related to the forward process) (Anderson, 1982; Haussmann & Pardoux, 1986) where θ denotes a parameter vector in a family of distributions $\mathcal{F}$ that q_0 belongs to. The equivalence (formalized in Proposition 1) suggests that maximizing the exact path likelihood of the reverse process is equivalent to maximizing the likelihood $\log q_0(\cdot; \theta)$.

To make it operational, we propose approximating the intractable reverse transition densities $p_{t-1|t}(Y_{t-1}|Y_t; \theta)$ via the Quasi-Maximum Likelihood Estimation (QMLE) with a proper Gaussian distributions (Wedderburn, 1974). As derived in Proposition 2, the mean and covariance of these conditional distributions depend not only on the score function $\nabla \log q_t(\cdot; \theta)$ but also on its Hessian function $\nabla^2 \log q_t(\cdot; \theta)$. We therefore parameterize both the score $s_t(\cdot; \phi)$ and the Hessian $H_t(\cdot; \phi)$ (e.g., using the neural networks) and optimize the parameters ϕ by minimizing the resulting approximate negative quasi-likelihood using the observed data trajectories.

Building upon this quasi-likelihood formulation, we introduce a computationally efficient objective called Likelihood Matching (LM). This objective not only provides a practical way to implement our framework but also offers a novel extension of the traditional score matching (SM), inherently incorporating covariance matching which is a form of likelihood weighting often beneficial in practice. Our key idea is summarized in Figure 1.

Recent works have incorporated likelihood information or higher-order terms into diffusion training, either via maximum-likelihood formulations for score-based models and diffusion ODEs (Song et al., 2021b; Lu et al., 2022; Zheng et al., 2023) or via Hessian-enhanced objectives (Dockhorn et al., 2021; Karras et al., 2022; Rissanen et al., 2024; Wang et al., 2025). However, these methods typically operate within regularized score-matching or probability-flow ODE formulations and thus still optimize surrogate objectives or upper bounds rather than the data likelihood itself. By contrast, we start from the exact path likelihood of the reverse diffusion SDE and construct an analytical quasi-maximum likelihood (QMLE) approximation of the reverse transition densities, yielding an LM objective that directly targets data likelihood.

Complementary to these continuous-time approaches, a closely related line of work in discrete-time DDPMs focuses on learning or designing the reverse covariance via variational objectives, including variance interpolation (Nichol & Dhariwal, 2021) and analytical ELBO-based derivations such as Analytic-DPM, SN-DDPM, and OCM-DDPM (Bao et al., 2022b; Ou et al., 2025; Bao et al., 2022a), as well as Gaussian mixture refinements (Guo et al., 2023). While these methods improve likelihood and sampling by better parameterizing the covariance within a fixed ELBO framework, LM is formulated in the continuous-time reverse SDE setting and uses QMLE to approximate the full path likelihood, providing a distinct likelihood-based training paradigm rather than a covariance-tuning strategy.

The main contributions of this work are the following

- We propose a novel training objective function for diffusion models based on the quasi-likelihood, leading to an approximation of the reverse path log-likelihood and a computationally efficient

variant called Likelihood Matching (LM) that combines score matching and covariance matching with implicit likelihood weighting.

- We derive a stochastic sampler that leverages both the learned score function and Hessian information through the implied conditional mean and covariance structure of transition densities.

- We provide non-asymptotic convergence guarantees for the proposed sampler in total variation distance, characterizing the errors in terms of score and Hessian estimation error, dimension d, and diffusion steps T. It reveals that the reverse step error scales at $O(d^3 \log^{4.5} T/T)$, while the score estimation error and Hessian estimation error are at the rate of $O(\sqrt{\log T})$ and $O(\log T/\sqrt{T})$, respectively.

- We theoretically demonstrate the consistency of the proposed quasi-maximum likelihood diffusion training under reverse quasi-likelihood objectives.

- We evaluate the proposed approach on standard benchmark image data, demonstrating its effectiveness and the impact of choices for Hessian approximation rank r and the number of distinct transition probability densities evaluated per sample path, confirming the critical role of the learned Hessian through ablation studies.

Detailed proofs of theoretical results are provided in Appendix B.

2 BACKGROUND AND MOTIVATIONS

2.1 NOTATIONS

Throughout the paper, we employ the following convention on notation: $\|\cdot\|$ designates the L_2 (spectral) norm for matrices or the L_2 norm for vectors, while $\|\cdot\|_F$ represents the Frobenius norm of a matrix. The determinant of a matrix is denoted by $|\cdot|$ or $\det(\cdot)$. For matrices A and B, we use $\mathrm{tr}(A)$ to represent the trace of A, and $A \succeq B$ indicates that $A - B$ is positive semidefinite. For two probability measure P and Q, we define their total-variation (TV) distance as $\mathrm{TV}(P\|Q) := \sup_{A \in \mathcal{F}} |P(A) - Q(A)|$ and their Kullback-Leibler (KL) divergence as $\mathrm{KL}(P\|Q) := \int \log(\mathrm{d}P/\mathrm{d}Q)\mathrm{d}P$. For two random vectors X and Y, $X \overset{d}{=} Y$ signifies that their cumulative distribution functions F_X and F_Y are identical almost surely. We employ $X_{0:t}$ to represent the sequence $(X_0, X_1, \cdots, X_t)$, $q_{s|t}$ denotes the conditional probability density function (PDF) of X_s given X_t and $q_{0:t}$ represents the joint PDF of $X_{0:t}$. We use $f(x) \lesssim g(x)$ or $f(x) = O(g(x))$ (resp. $f(x) \gtrsim g(x)$) to denote $f(x) \leq cg(x)$ (resp. $f(x) \geq cg(x)$) for a universal constant c and all x. We write $f(x) \asymp g(x)$ when both $f(x) \lesssim g(x)$ and $f(x) \gtrsim g(x)$ hold.

2.2 PRELIMINARIES AND MOTIVATIONS

We adhere to the foundational generative models introduced in Song et al. (2021c), where both the forward and reverse processes are characterized by a unified system of stochastic differential equations (SDEs).

Let $X_1, \cdots, X_n$ be independent and identically distributed (IID) random observations from a target distribution on $\mathbb{R}^d$ with density q_0. We assume this distribution belongs to a specific parametric family of distributions $\mathcal{F}_\theta$, characterized by a true parameter $\theta \in \mathbb{R}^h$, with the PDF $q_0(\theta)$. The high dimensionality of θ often presents challenges for traditional statistical inference methods, highlighting a key area where diffusion models can provide better solutions.

The forward diffusion process for $\{X_t\}_{t \in [0,T]}$ in $\mathbb{R}^d$ is expressed by SDEs

$$\mathrm{d}X_t = -\frac{1}{2}\beta_t X_t \mathrm{d}t + \sqrt{\beta_t}\mathrm{d}W_t, \quad X_0 \sim q_0(\theta), \tag{1}$$

where β_t is a given time-dependent diffusion coefficient and W_t denotes the Brownian motion. Let $q_t(\cdot; \theta)$ represents the PDF of X_t. It is noted that $q_t(\cdot; \theta)$ only depend on θ since the transition density $q_{t|t-1}$ is free of the parameter θ as β_t is known.

Under mild regularity conditions on $q_0(\theta)$, Anderson (1982) and Haussmann & Pardoux (1986) establish that there are reverse-time SDEs $\{Y_t\}_{t \in [T,0]}$ which exhibit identical marginal distributions

as the forward diffusion processes (1) such that $Y_t \overset{d}{=} X_t$, and satisfy

$$\mathrm{d}Y_t = \frac{1}{2}\beta_t(Y_t + 2\nabla \log q_t(Y_t; \theta))\mathrm{d}t + \sqrt{\beta_t}\mathrm{d}\bar{W}_t, \quad Y_T \sim q_T(\theta), \tag{2}$$

where $\bar{W}_t$ is the Brownian motion, $p_t(\cdot; \theta)$ is the PDF of Y_t and $\nabla \log q_t(\cdot; \theta)$ represents the score function of the marginal density q_t. As both θ and q_t are unknown, the exact score function is inaccessible. Therefore, we endeavor to approximate it with a suitable estimator $s_t(\cdot)$. Typically, we parametrize $s_t(\cdot)$ as $s_t(\cdot; \phi)$ via either a neural network (or parametric models like the Gaussian Mixtures) base on the sample $\{X_i\}_{i=1}^n$. To be precise, throughout this paper, θ refers to the true parameters of the data distribution in an oracle setting (i.e., when the parametric family $\mathcal{F}_\theta$ is known), whereas ϕ denotes the learnable parameters of our neural network models.

Additionally, we substitute the distribution of Y_T with a prior distribution π, which is specifically chosen as $\mathcal{N}_d(0, I_d)$ to facilitate data generation. Consequently, the modified reverse diffusion process $\{\hat{Y}_t\}_{t \in [T, 0]}$ is defined as

$$\mathrm{d}\hat{Y}_t = \frac{1}{2}\beta_t(\hat{Y}_t + 2s_t(\hat{Y}_t; \phi))\mathrm{d}t + \sqrt{\beta_t}\mathrm{d}\bar{W}_t, \quad \hat{Y}_T \sim \pi = \mathcal{N}_d(0, I_d). \tag{3}$$

The existing approach matches the score function $\nabla \log q_t(X_t)$ with an objective function (Hyvärinen & Dayan, 2005; Song et al., 2020), which aims to learn the score function by minimizing

$$\mathcal{J}_{\mathrm{SM}}(\phi) := \frac{1}{2}\int_0^T \mathbb{E}_{X_0 \sim q_0}\mathbb{E}_{X_t \sim q_{t|0}}\left[\lambda(t)\left\|\nabla \log q_t(X_t|X_0) - s_t(X_t; \phi)\right\|^2\right]\mathrm{d}t + \tilde{C}_T, \tag{4}$$

where $\lambda(t)$ is a positive weighting function and $s_t(X_t; \phi)$ is an neural network (NN) with parameter ϕ. The rationale for the approach is the following inequality (Corollary 1 in Song et al. (2021b)):

$$-\mathbb{E}_{X_0}\left[\log q_0(X_0; \phi)\right] \leq \mathcal{J}_{\mathrm{SM}}(\phi) + C_1, \tag{5}$$

where C_1 is a constant independent of ϕ. This inequality explicitly shows that classical score matching only minimizes an upper bound on the negative log-likelihood rather than the likelihood itself. However, recent analyses (Koehler et al., 2023) have shown that this can lead to a severe loss of statistical efficiency compared to MLE, even for simple families of distributions like exponential families. Motivated by this limitation, we propose an approach that directly minimizes the negative log-likelihood $-\mathbb{E}_{X_0}\left[\log q_0(X_0; \phi)\right]$ instead of its upper bound $\mathcal{J}_{\mathrm{SM}}$.

To derive the relationship between the likelihood of forward and backward trajectories, by a property of reversal diffusion (Haussmann & Pardoux, 1986), for any chosen time steps $0 = t_0 < t_1 < \cdots < t_{N-1} < t_N = T$, there is an equivalence of the joint likelihoods between the forward and the reverse processes:

$$q_{t_0:t_N}(x_{t_0}, x_{t_1}, \cdots, x_{t_N}; \theta) = p_{t_0:t_N}(x_{t_0}, x_{t_1}, \cdots, x_{t_N}; \theta), \tag{6}$$

where $q_{t_0:t_N}$ and $p_{t_0:t_N}$ represent the joint densities of the processes $\{X_{t_k}\}_{k=0}^N$ and $\{Y_{t_k}\}_{k=0}^N$.

The following proposition shows that the expected log-likelihood at $t = 0$ can be expressed by transition and marginal densities of the forward and the time-reversal processes. It will serve to construct the wanted likelihood approximation.

Proposition 1. *Suppose that there exits a positive constant C such that $0 < \beta_t \leq C$ for any $t \in [0, T]$, and for any open bounded set $\mathcal{O} \subseteq \mathbb{R}^d$, $\int_0^T \int_{\mathcal{O}}(\|q_t(x; \theta)\|^2 + d \cdot \beta_t \|\nabla q_t(x; \theta)\|^2)\mathrm{d}x\mathrm{d}t < \infty$, then*

$$\mathbb{E}_{X_{t_0} \sim q_{t_0}} \log q_{t_0}(X_{t_0}; \theta) = \mathbb{E}_{X_{t_0:t_N} \sim q_{t_0:t_N}}\left\{\sum_{k=1}^N \log p_{t_{k-1}|t_k}(X_{t_{k-1}}|X_{t_k}; \theta)\right.$$

$$\left. + \log \underbrace{p_{t_N}(X_{t_N}; \theta)}_{\text{converge to } \mathcal{N}_d(0, I_d)} - \sum_{k=1}^N \log \underbrace{q_{t_k|t_{k-1}}(X_{t_k}|X_{t_{k-1}})}_{\text{given by (1) (independent of } \theta)}\right\} \tag{7}$$

for any $0 < t_1 < \cdots < t_{N-1} < T$.

4

Proposition 1 links the expected log-likelihood of the initial distribution to that involving the forward process and the reverse process. As the forward transition density $q_{t_k|t_{-1}}(X_{t_k}|X_{t_{k-1}})$ is free of the parameter θ due to β_t being known, and for sufficiently large t_N, the density $p_{t_N}(X_{t_N};\theta)$ converges to a stationary distribution $\mathcal{N}_d(0, I_d)$ that is also independent of θ, (7) becomes

$$-\mathbb{E}_{X_0 \sim q_0}[\log q_0(X_0;\theta)] \approx -\mathbb{E}_{X_{t_0:t_N} \sim q_{t_0:t_N}} \Big\{ \sum_{k=1}^{N} \log p_{t_{k-1}|t_k}(X_{t_{k-1}}|X_{t_k};\theta) \Big\} + C_T$$

$$=: \mathcal{L}(\theta) + C_T, \tag{8}$$

where C_T denotes a constant free of θ.

The approximation in (8) arises from using a finite terminal time T instead of infinity. This truncation error is well-controlled; as established in Appendix B (Lemma 1), the KL divergence between the perturbed data distribution q_T and the prior distribution converges to zero at a polynomial rate with respect to T. Expression (8) suggests a more attractive strategy, that is to minimize a computable version of $\mathcal{L}(\theta)$ rather than minimizing a version of the upper bound $\mathcal{J}_{\text{SM}}(\phi)$ in (5). In the next section, we detail an approach using the Quasi Maximum Likelihood, which allows constructing a tractable objective function by specifying an analytical form for these conditional log-likelihood terms.

Moreover, the arbitrariness of $t_1 < \cdots < t_{N-1}$ in (7) offers convenience for designing efficient algorithms to realize the approximation of $\mathcal{L}(\theta)$.

3 METHODOLOGY

We assume access to the original data $\{X_0^{(i)}\}_{i=1}^n$ where each $X_0^{(i)} \in \mathbb{R}^d$ at $t = 0$. For any fixed index i, we can generate a sequence of discrete observations $\{X_{t_k}^{(i)}\}_{k=0}^N$ according to the SDEs (1). Throughout the paper, we denote by $T > 0$ the diffusion horizon of the continuous-time SDE, and by N the number of discrete reverse transition densities evaluated per path in the LM objective. In the theoretical analysis (Section 4) we set $t_k = k$ and $N = T$ with unit time increments, while in the experiments (Section 5) we draw a random grid of N time points from $[0, T]$ as in Algorithm 2.

3.1 QUASI-MAXIMUM LIKELIHOOD ESTIMATION

The objective function $\mathcal{L}(\theta)$ requires evaluating the transition densities $p_{t_{k-1}|t_k}(Y_{t_{k-1}}|Y_{t_k};\theta)$, whose functional forms are unavailable. We adopt the Quasi-Maximum Likelihood approach (QML) (Wedderburn, 1974). This involves replacing the intractable true reverse transition density $p_{t_{k-1}|t_k}$ with a tractable proxy. Specifically, we use a Gaussian distribution whose mean and covariance match the true conditional mean and covariance of the reverse process, which are derived in Proposition 2. As $Y_t \stackrel{d}{=} X_t$ and the joint PDF equivalence (6), these moments are the same as those of $q_{t_{k-1}|t_k}(X_{t_{k-1}}|X_{t_k};\theta)$.

The following proposition provides the analytical forms of these conditional mean and covariance, which are used to define matched Gaussian distribution in the quasi-likelihood.

Proposition 2. *Let $\mu_{s|t}$ and $\Sigma_{s|t}$ be the conditional mean and covariance of $q_{s|t}(X_s|X_t;\theta)$, respectively, for $s < t$. Then,*

$$\mu_{s|t} = \mathbb{E}\left(X_s|X_t\right) = \frac{X_t + \sigma_{t|s}^2 \nabla \log q_t(X_t;\theta)}{m_{t|s}} \quad and$$

$$\Sigma_{s|t} = \mathbb{E}\left[\left(X_s - \mu_{s|t}\right)\left(X_s - \mu_{s|t}\right)^T |X_t\right] = \frac{\sigma_{t|s}^2}{m_{t|s}^2}\left(I_d + \sigma_{t|s}^2 \nabla^2 \log q_t(X_t;\theta)\right),$$

where $m_{t|s} = \exp\{-\int_s^t \beta_t \mathrm{d}t/2\}$ and $\sigma_{t|s}^2 = 1 - \exp\{-\int_s^t \beta_t \mathrm{d}t\}$.

To facilitate the QMLE approach, we parameterize both $\nabla \log q_t(X_t;\theta)$ and the Hessian function $\nabla^2 \log q_t(X_t;\theta)$. This parameterization strategy adapts to whether the data's parametric family $\mathcal{F}_\theta$ is known a priori. In specialized domains like financial modeling or signal processing, where $\mathcal{F}_\theta$ can be

known, these functions can be expressed analytically in terms of the true parameters θ, a property we use for parameter estimation in Section 5.1. More commonly, for complex high-dimensional data like images where $\mathcal{F}_\theta$ is unknown, we employ neural networks as universal approximators. Our implementation uses two separate U-Net models to represent the score $s_t(x; \phi)$ and the Hessian $H_t(x; \phi)$, where ϕ denotes their learnable parameters.

The quasi-likelihood approximation to transition density $p_{t_{k-1}|t_k}(Y_{t_{k-1}}|Y_{t_k}; \phi)$ is

$$\hat{p}_{t_{k-1}|t_k}(Y_{t_{k-1}}|Y_{t_k}; \phi) = \varphi_d(Y_{t_{k-1}}; \mu_{t_{k-1}|t_k}(Y_{t_k}; \phi), \Sigma_{t_{k-1}|t_k}(Y_{t_k}; \phi)), \tag{9}$$

where $\varphi_d(x; \mu, \Sigma)$ denote the d-dimensional Gaussian density with mean μ and covariance Σ, $\mu_{t_{k-1}|t_k}(Y_{t_k}; \phi) = m_{t_k|t_{k-1}}^{-1}(Y_{t_k} + \sigma_{t_k|t_{k-1}}^2 s_{t_k}(Y_{t_k}; \phi))$ and $\Sigma_{t_{k-1}|t_k} = m_{t_k|t_{k-1}}^{-2} \sigma_{t_k|t_{k-1}}^2 \{I_d + \sigma_{t_k|t_{k-1}}^2 H_{t_k}(Y_{t_k}; \phi)\}$. With the quasi-Gaussian specification (9), we define the population-level quasi-log-likelihood objective function

$$\mathcal{L}(\phi) = -\sum_{k=1}^N \mathbb{E}_{X_{t_0:t_N} \sim q_{t_0:t_N}} \{\log \hat{p}_{t_{k-1}|t_k}(X_{t_{k-1}}|X_{t_k}; \phi)\} \tag{10}$$

based on the forward data processes by noting (7) and (9).

Let $\ell_{\{t_0,\cdots,t_N\}}^{(i)}(\phi) = -\sum_{k=1}^N \log \hat{p}_{t_{k-1}|t_k}(X_{t_{k-1}}^{(i)}|X_{t_k}^{(i)}; \phi)$, where $X_{t_k}^{(i)} = m_{t_k|t_{k-1}} X_{t_{k-1}}^{(i)} + \sigma_{t_k|t_{k-1}} Z_{t_k}^{(i)}$ be the realized path of the forward SDE (1) and $\{Z_{t_k}^{(i)}\}_{k=1}^N$ are IID standard Gaussian noise, and let

$$\mathcal{J}_{n,N}(\phi) = n^{-1} \sum_{i=1}^n \ell_{\{t_0,\cdots,t_N\}}^{(i)}(\phi) \tag{11}$$

be the aggregated sample quasi-log-likelihood, which depends on the choices of $\{t_0, t_1, \cdots, t_N\}$. Let $\hat{\phi}_{n,N} = \arg\min_\phi \mathcal{J}_{n,N}(\phi)$ be the quasi-MLE. Substituting $s_t(Y_t; \hat{\phi}_{n,N})$ to the reverse SDE (2) yields the modified reverse SDE

$$d\hat{Y}_t = \frac{1}{2}\beta_t(\hat{Y}_t + 2s_t(\hat{Y}_t; \hat{\phi}_{n,N}))dt + \sqrt{\beta_t}d\bar{W}_t, \quad \hat{Y}_T \sim \pi = \mathcal{N}_d(0, I_d), \tag{12}$$

and denote the density of of $\hat{Y}_t(\hat{\phi}_{n,N})$ by $p_t(\cdot; \hat{\phi}_{n,N})$. For notational simplicity, in the rest of this paper, we use $q_t \equiv q_t(\cdot; \theta)$, $\hat{p}_t \equiv p_t(\cdot; \hat{\phi}_{n,N})$, $\hat{s}_t(\cdot) \equiv s_t(\cdot; \hat{\phi}_{n,N})$ and $\hat{H}_t(\cdot) \equiv H_t(\cdot; \hat{\phi}_{n,N})$.

Stochastic Sampler. Proposition 2 implies the following sampling procedure that differs from the conventional DDPM-type sampler (Ho et al., 2020):

$$\tilde{Y}_{t-1} = \hat{\mu}_{t-1|t}(\tilde{Y}_t) + \hat{\Sigma}_{t-1|t}^{\frac{1}{2}}(\tilde{Y}_t)Z_t \tag{13}$$

for $t = T, \cdots, 1$, where $Z_t \overset{\text{IID}}{\sim} \mathcal{N}_d(0, I_d)$ and

$$\begin{aligned}
\hat{\mu}_{t-1|t}(\tilde{Y}_t) &= m_{t|t-1}^{-1}(\tilde{Y}_t + \sigma_{t|t-1}^2 \hat{s}_t(\tilde{Y}_t)), \\
\hat{\Sigma}_{t-1|t}(\tilde{Y}_t) &= m_{t|t-1}^{-2} \sigma_{t|t-1}^2 \{I_d + \sigma_{t|t-1}^2 \hat{H}_t(\tilde{Y}_t)\},
\end{aligned} \tag{14}$$

which involves the score and the Hessian function. Similarly, we denote the PDF of $\tilde{Y}_t$ generated by (13) as $\tilde{p}_t$. An efficient implementation of the sampling scheme is given in Appendix C.4.

3.2 LIKELIHOOD MATCHING AND EFFICIENT ALGORITHMS

To realize the Quasi-Likelihood (11), the intermediate time points t_1 through t_{N-1} are fixed in advance. To effectively utilize the evolutionary information from the forward SDEs, practitioners often employ an exceedingly large number of discretization steps, say N, to generate training data. However, such fine-grained discretization imposes significant computational burdens on training both the score model s_t and the Hessian model H_t. To address this issue, we propose a more efficient computational algorithm.

We note that that Proposition 1 holds true for arbitrary time points $0 < t_1 < \cdots < t_{N-1} < T$, which enables a time-averaged version of (10), expressed as:

$$-\frac{(N-1)!}{T^{N-1}} \int_0^T \cdots \int_0^{t_2} \sum_{k=1}^N \mathbb{E}_{X_{t_0:t_N} \sim q_{t_0:t_N}} \left\{ \log \hat{p}_{t_{k-1}|t_k}(X_{t_{k-1}}|X_{t_k}; \phi) \right\} \mathrm{d}t_1 \cdots \mathrm{d}t_{N-1}.$$

An empirical version can be constructed by randomly sampling an ordered time grid $(t_1^{(i)}, \cdots, t_{N-1}^{(i)})$ from the uniform distribution over the simplex $\mathcal{T} = \{(t_1, \cdots, t_{N-1}) \in (0, T)^{N-1} \mid t_1 < \cdots < t_{N-1}\}$, yielding the following stochastic optimization objective

$$\tilde{J}_{n,N}(\phi) = n^{-1} \sum_{i=1}^n \ell_{\{t_0, t_1^{(i)}, \cdots, t_{N-1}^{(i)}, t_N\}}^{(i)}(\phi) = n^{-1} \sum_{i=1}^n \sum_{k=1}^N \{-\log \hat{p}_{t_{k-1}^{(i)}|t_k^{(i)}}(X_{t_{k-1}^{(i)}}^{(i)}|X_{t_k^{(i)}}^{(i)}; \phi)\},$$
(15)

where

$$-\log \hat{p}_{t_{k-1}^{(i)}|t_k^{(i)}}(X_{t_{k-1}^{(i)}}^{(i)}|X_{t_k^{(i)}}^{(i)}; \phi)$$
$$= \frac{1}{2} \log |\Sigma_{t_{k-1}^{(i)}|t_k^{(i)}}(X_{t_k^{(i)}}^{(i)}; \phi)| + \frac{1}{2} \|\Sigma_{t_{k-1}^{(i)}|t_k^{(i)}}^{-\frac{1}{2}}(X_{t_k^{(i)}}^{(i)}; \phi)(X_{t_{k-1}^{(i)}}^{(i)} - \mu_{t_{k-1}^{(i)}|t_k^{(i)}}(X_{t_k^{(i)}}^{(i)}; \phi))\|^2. \quad (16)$$

We call (15) the Likelihood Matching (LM) objective. The random time-point selection strategy allows a more comprehensive temporal evaluation during training, even with a modest transition step N. Regarding the time sampling strategy, our objective in (15) is derived from the path integral of the log-likelihood (Proposition 1), which implies a uniform integration over time. Consequently, sampling uniformly from the simplex yields an unbiased Monte Carlo estimator. While prior works often employ hand-crafted, non-uniform sampling schemes to emphasize difficult noise levels (Song et al., 2021c; Karras et al., 2022), incorporating such schedules into LM would require importance weighting to maintain unbiasedness. Exploring importance sampling or non-uniform weighting within the LM framework to reduce gradient variance remains an interesting direction for future work.

Furthermore, by expanding equation (16), the second term in (16) becomes

$$\frac{1}{2} \|(I_d + \sigma_{t_k^{(i)}|t_{k-1}^{(i)}}^2 H_{t_k^{(i)}}(X_{t_k^{(i)}}^{(i)}; \phi))^{-\frac{1}{2}}(Z_{t_k^{(i)}} + \sigma_{t_k^{(i)}|t_{k-1}^{(i)}} s_{t_k^{(i)}}(X_{t_k^{(i)}}^{(i)}; \phi))\|^2$$

which unifies the score matching (Song et al., 2021c) and likelihood weighting (Song et al., 2021b) as special cases of the transition probability within our LM objective. In particular, when $\hat{H}_t \equiv 0$ the second term reduces to a rescaled ℓ_2 loss between $Z_{t_k^{(i)}}$ and $\sigma_{t_k^{(i)}|t_{k-1}^{(i)}} s_{t_k^{(i)}}(X_{t_k^{(i)}}^{(i)}; \phi)$, recovering standard score matching; the presence of $(I + \sigma^2 H_t)^{-1/2}$ plays the role of an automatically learned likelihood weight, while the extra $\log |\Sigma_{t_{k-1}|t_k}|$ term completes a proper quasi likelihood for the reverse transition. However, our formulation integrates covariance to weight the score while leveraging additional transition probabilities, thereby utilizing more trajectory information. The algorithm for Likelihood Matching is provided in Appendix A.

The LM objective (15) incorporates both score matching and an additional covariance matching. Moreover, it naturally weights each time step via the matched covariance, rather than relying on pre-specified weights, for instance, $\lambda(t)$ in (4). The experimental section analyzes how different number of generated time points N in (15) affects the performance.

Exploiting the intrinsic dimensionality of real data distributions, Meng et al. (2021) proposed parameterizing $H_t(X_t; \phi)$ with low-rank matrices defined as $H_t(X_t; \phi) = U_t(X_t; \phi) + V_t(X_t; \phi)V_t(X_t; \phi)^T$ where $U_t(\cdot; \phi) : \mathbb{R}^d \to \mathbb{R}^{d \times d}$ is a diagonal matrix, and $V_t(\cdot; \phi) : \mathbb{R}^d \to \mathbb{R}^{d \times r}$ is a matrix with a prespecified rank $r \ll d$ for a pre-determined r, reducing computational complexity. We explore the impact of different r in the experimental section.

To efficiently compute the likelihood (15), we apply the Sherman-Morrison-Woodbury (SMW) formula, namely after suppressing argument $(X_t; \phi)$ in related quantities, for any $X \in \mathbb{R}^d$,

$$X^T(I_d + \sigma_{t_{k-1}|t_k}^2 U_t + \sigma_{t_{k-1}|t_k}^2 V_t V_t^T)^{-1} X = \tilde{X}^T \tilde{X} - (\tilde{V}_t^T \tilde{X})^T (I_r + \tilde{V}_t^T \tilde{V}_t)^{-1}(\tilde{V}_t^T \tilde{X}),$$

where $\tilde{X} = (I_d + \sigma^2_{t_{k-1}|t_k} \boldsymbol{U}_t)^{-1/2} X$ and $\tilde{\boldsymbol{V}}_t = \sigma_{t_{k-1}|t_k} (I_d + \sigma^2_{t_{k-1}|t_k} \boldsymbol{U}_t)^{-1/2} \boldsymbol{V}_t$. Similarly, the determinant can be computed efficiently using the matrix determinant lemma:

$$|I_d + \sigma^2_{t_{k-1}|t_k} \boldsymbol{U}_t + \sigma^2_{t_{k-1}|t_k} \boldsymbol{V}_t \boldsymbol{V}_t^T| = |I_d + \sigma^2_{t_{k-1}|t_k} \boldsymbol{U}_t| \cdot |I_r + \tilde{\boldsymbol{V}}_t \tilde{\boldsymbol{V}}_t^T|.$$

More details are in the Appendix C.4.

4 THEORETICAL ANALYSIS

In the theoretical analysis, we set $t_k = k$ and $N = T$, and specify the noise schedule β_t similar to Li et al. (2023) (details in Appendix B), and assume the following assumptions.

Assumption 1 (Boundedness of the Distribution). *The original data distribution q_0 possesses a bounded second-order moment such that $\mathbb{E}_{X \sim q_0} \|X\|^2 \leq M_2$ for a positive constant M_2.*

Assumption 2 (L_2 Score Estimation Error). *The estimated score function $\hat{s}_t(x)$ satisfies $T^{-1} \sum_{t=1}^T \mathbb{E}_{X \sim q_t} \|\nabla \log q_t(X) - \hat{s}_t(X)\|^2 \leq \varepsilon_s^2$ for a constant $\varepsilon_s > 0$.*

Assumption 3 (Frobenius Hessian Estimation Error). *The estimated Hessian function $\hat{H}_t(x)$ satisfies $T^{-1} \sum_{t=1}^T \mathbb{E}_{X \sim q_t} \|\nabla^2 \log q_t(X) - \hat{H}_t(X)\|_F^2 \leq \varepsilon_H^2$ for a constant $\varepsilon_H > 0$.*

Assumption 4. *The true Hessian function $\nabla^2 \log q_t(x)$ satisfies $\lambda_{\min}((1 - \alpha_t)\nabla^2 \log q_t(x)) \geq \varepsilon_0 > -1$, where ε_0 is constant.*

Assumption 1-3 are standard in the literature (Li et al., 2023; 2024; Benton et al., 2023; Chen et al., 2023). Assumption 4 is relatively mild. By Proposition 2, we know that $I_d + (1 - \alpha_t)\nabla^2 \log q_t(x) \succeq 0$, which implies that all eigenvalues of $(1 - \alpha_t)\nabla^2 \log q_t(x)$ must be greater than or equal to -1.

Theorem 1 (Non-asymptotic Bound for Distributions with Bounded Moments). *Under Assumptions 1-4, the generated distribution $\tilde{p}_0$ by Sampler (13) satisfies*

$$\mathrm{TV}(q_0 \| \tilde{p}_0) \leq \sqrt{\frac{1}{2} \mathrm{KL}(q_0 \| \tilde{p}_0)} \lesssim \frac{d^3 \log^{4.5} T}{T} + \sqrt{\log T} \varepsilon_s + \frac{\log T}{\sqrt{T}} \varepsilon_H. \tag{17}$$

Theorem 1 provides non-asymptotic convergence guarantees for the stochastic sampler (13). The error bound consists of three terms: the reverse step error that scales as $O(d^3 \log^{4.5} T/T)$, reflecting the discrepancy between forward and reverse transition densities; the score estimation error and Hessian estimation errors which are $O(\sqrt{\log T})$ and $O(\log T/\sqrt{T})$, respectively, due to utilization of mean and covariance information in the sampling procedure. To achieve the ε-accuracy approximation error, assuming the exact score, the total number of time steps T should be $O(d^3/\varepsilon)$.

In the following theorem, we consider an oracle parametric setting where the score can be written as $s_t(x; \theta) = \nabla \log q_t(x; \theta)$ for a finite-dimensional parameter θ. Thus, unlike the nonparametric neural-network setting where we denote network weights by ϕ, here θ directly indexes the data-generating family $\mathcal{F}_\theta$.

Theorem 2 (Consistency under Oracle Model). *Suppose $s_t(x; \theta) = \nabla \log q_t(x; \theta)$ for any $t \geq 0$. Then, under conditions given in the Appendix B.4, the quasi-MLE $\hat{\theta}_{n,T} \xrightarrow{p} \theta^*$ in probability as $n, T \to \infty$, where θ^* is the parameter of the original data distribution q_0.*

The theorem shows that when the true form of the score function is accessible, the estimation by minimizing the Likelihood Matching objective (15) converges to the true value.

5 EXPERIMENTS

This section reports empirical results to validate our theory and methodological insights through numerical experiments on both synthetic datasets and image datasets. To ensure the reproducibility of our results, we provide a comprehensive description of all experimental details, including experiment setting, additional results, and an analysis of the computational time and memory consumption, in Appendix C.
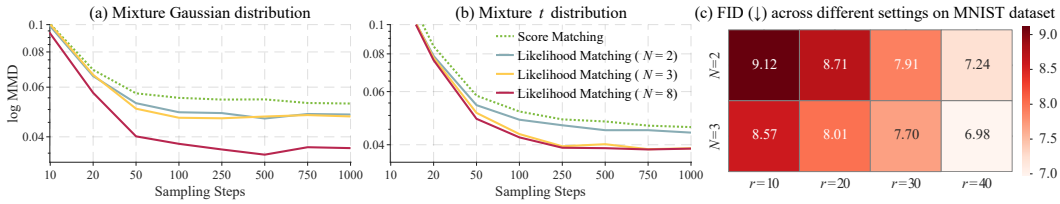
Figure 2: Maximum Mean Discrepancy (MMD; lower is better) between generated and true samples under two 1D mixture distributions: (a) Gaussian and (b) t with 3 degrees of freedom with respect to the number of sampling steps N. (c) Fréchet Inception Distance (FID; lower is better) on the MNIST dataset for different combinations of (N, r) under the Likelihood Matching framework.

5.1 Synthetic datasets

Mixture Model. To analyze a known failure case of Score Matching, which can struggle to accurately fit mixture distributions with well-separated modes (Koehler et al., 2023), we first considered a two-component Gaussian mixture with equal weights and means located at -10 and 10, with unit variance. We also examined mixtures of the t-distributions with 3 degrees of freedom under the same settings. We used a single-hidden-layer multilayer perceptron (MLP) to model both the score and Hessian functions, and compared the performance of the Score Matching method with the Likelihood Matching method using transition step $N = 2$, 3, and 8. For evaluation, we used the Maximum Mean Discrepancy (MMD, Gretton et al. 2012), which employed five Gaussian kernels with bandwidths $\{2^{-2}, 2^{-1}, 2^0, 2^1, 2^2\}$. The results, averaged over 100 independent trials, are reported in Figures 2 (a)-(b), which show that the proposed LM consistently outperformed the Score Matching, and the performance of the LM improved as N increases.

Parameter Estimation. We evaluated the LM approach on a two-dimensional Gaussian mixture distribution, i.e., $q_0(x) \sim \omega_1 \mathcal{N}_2(\mu_1, \sigma_1^2 I_2) + (1 - \omega_1) \mathcal{N}_2(\mu_2, \sigma_2^2 I_2)$, where the score model (with the true oracle score) can be derived analytically. Using ground truth parameters $\mu_1 = (1, 2)^T$, $\mu_2 = (-1, -3)^T$, $\sigma_1 = \sqrt{0.3}$, $\sigma_2 = \sqrt{0.6}$ and $\omega_1 = 1/3$, we compared parameter estimation between the Likelihood Matching (LM) and Score Matching methods. For sample sizes $n = 100$ and 200 (500 replicates each), we report the mean absolute error (MAE) and standard error (Std. Error) in Table 2 (Appendix C.2), which showed that the LM had consistently lower MAE and Std. Error than the Score Matching. The decreasing estimation variance of the LM with increasing sample size supported the consistency guarantee in Theorem 2.

5.2 Image datasets

The performance of the Likelihood Matching is expected to improve as both N and r increase. To verify this, we trained the Likelihood Matching model on the MNIST dataset under different settings of (N, r). The FID (Fréchet Inception Distance) for each setting is presented in Figure 2 (c), which aligns well with the expectation.

We evaluated our LM framework on the CIFAR-10 and CelebA 64x64 datasets, comparing it against a SM baseline. As shown in Table 1, the LM method consistently outperforms SM across all metrics. Notably, even with a simple diagonal Hessian approximation ($r = 0$), LM achieves a lower FID on both CIFAR-10 (3.12 vs. 3.15) and CelebA (2.69 vs. 2.71), alongside improved negative log-likelihood (NLL) where the NLL metric is computed directly in the discrete SDE formulation by evaluating the exact Gaussian likelihood of the residuals under the learned covariance, as detailed in Appendix C.

The performance gains become more significant as the rank of the Hessian approximation increases, peaking around $r = 20 - 30$. This demonstrates a clear benefit from incorporating covariance information. For instance, LM with $r = 30$ achieves a FID of 3.03 on CIFAR-10 and 2.62 on CelebA, a notable improvement over the SM baseline. These results provide strong empirical evidence that our likelihood-based objective is fundamentally more effective than score matching for training high-fidelity generative models.

We then performed sampling on the MNIST dataset using the sampler described (13) based on the trained Likelihood Matching ($N = 2, r = 10$) and the Score Matching, where the Hessian function in Score Matching is fixed as zero. Both methods perform well with a large number of sampling steps.

Table 1: Quantitative comparison on CIFAR-10 and CelebA 64x64. LM with fixed transition steps ($N = 2$) and varying Hessian ranks (r) is compared against the Score Matching (SM) baseline. FID ($\downarrow$) and NLL ($\downarrow$) indicate lower is better, while IS ($\uparrow$) indicates higher is better.

	CIFAR10 FID $\downarrow$	CIFAR10 IS $\uparrow$	CIFAR10 NLL (bpd) $\downarrow$	CelebA 64×64 FID $\downarrow$
SM	3.15	9.47 ± 0.10	3.28	2.71
LM ($r = 0$)	3.12	9.47 ± 0.11	3.24	2.69
LM ($r = 10$)	3.04	9.46 ± 0.13	3.15	2.67
LM ($r = 20$)	**3.01**	$\mathbf{9.48 \pm 0.14}$	3.13	2.65
LM ($r = 30$)	3.03	9.45 ± 0.13	**3.11**	**2.62**
LM ($r = 100$)	3.05	9.46 ± 0.12	3.12	2.63
LM ($r = 200$)	3.09	9.46 ± 0.15	3.13	2.64

Figure 4 (Appendix C.2) presents the results under fewer sampling steps, where we observe that Likelihood Matching exhibits faster convergence and better preservation of the structural integrity of the generated images. Qualitatively, after only 20 reverse iterations the LM sampler already produces clearly recognizable digits, whereas the corresponding SM samples remain noticeably more blurred and less structured, indicating that the Hessian-based covariance improves the per-step accuracy of the reverse transition and effectively reduces the number of sampling steps needed to reach a given visual quality.

A more detailed analysis of training and sampling time, as well as GPU memory usage, is given in Appendix C. In particular, Table 3 reports the overhead on CIFAR-10, while Table 4 shows that on 224×224 ImageNet our method increases training time by roughly 3–4$\times$ and memory by about 2–3$\times$ over the SM baseline, confirming both the scalability challenge and the current computational feasibility of LM.

5.3 ABLATION STUDIES

Marginal Benefit of Hessian. To isolate the contribution of the learned Hessian, we conducted an ablation study on MNIST where the score network was trained but the Hessian was set to a fixed identity matrix $H_t \equiv I$. This score-only LM variant resulted in significantly worse FID scores (10.28 for $N = 2$ and 9.75 for $N = 3$) compared to the full LM model, confirming that explicitly modeling the covariance is crucial for performance. Empirically, we find that relatively small ranks yield the best trade-off between performance and computational cost. As shown in Table 1, moving from a diagonal Hessian ($r = 0$) to $r = 20\text{-}30$ brings noticeable gains, while higher ranks ($r = 100, 200$) offer diminishing returns. Therefore, we recommend $r \in [10, 30]$ as a practical guideline for standard image benchmarks.

6 CONCLUSION

This work introduces the Likelihood Matching method for training diffusion models, which is grounded in the Maximum Likelihood Estimation, by leveraging on the Quasi-Maximum Likelihood Estimation (QMLE). The approach inherently integrates both score and covariance matching, distinguishing it from the score matching that focuses solely on a single transition density and utilizes only the first-order moment information. Our theoretical analysis establishes the consistency of the QMLE and provides non-asymptotic convergence guarantees for the proposed sampler quantifying the impact of the score and Hessian estimation errors, dimensionality, and diffusion steps. Empirical evaluations on image datasets demonstrated the viability of the proposed approach and elucidated the influence of methodological choices such as Hessian approximation rank. Our comprehensive evaluations show that LM consistently outperforms the foundational SM baseline in generation quality and likelihood estimation, with a manageable and scalable increase in computational cost.

Building upon this robust foundation, future directions involve exploring the application of our methods to more challenging, high-dimensional data domains, such as high-resolution natural images or video generation. Concurrently, enhancing the computational efficiency of both the training and sampling procedures represents another promising avenue for further research, aimed at broadening the practical applicability of LM. In particular, the computational burden of Hessian modeling on

large-scale datasets remains substantial, and alleviating this limitation is an important direction for future work. Our LM objective is also complementary to the rich body of work on optimal covariance design and non-Gaussian transition approximations in diffusion models, and combining LM with such advanced solvers on large-scale benchmarks such as ImageNet is an especially promising direction.

REFERENCES

Brian DO Anderson. Reverse-time diffusion equation models. *Stochastic Processes and their Applications*, 12(3):313–326, 1982.

Fan Bao, Chongxuan Li, Jiacheng Sun, Jun Zhu, and Bo Zhang. Estimating the optimal covariance with imperfect mean in diffusion probabilistic models. In *International Conference on Machine Learning*, pp. 1555–1584. PMLR, 2022a.

Fan Bao, Chongxuan Li, Jun Zhu, and Bo Zhang. Analytic-DPM: an analytic estimate of the optimal reverse variance in diffusion probabilistic models. In *International Conference on Learning Representations*, 2022b.

Joe Benton, Valentin De Bortoli, Arnaud Doucet, and George Deligiannidis. Nearly d-linear convergence bounds for diffusion models via stochastic localization. *International Conference on Learning Representations*, 2023.

James Betker, Gabriel Goh, Li Jing, Tim Brooks, Jianfeng Wang, Linjie Li, Long Ouyang, Juntang Zhuang, Joyce Lee, Yufei Guo, et al. Improving image generation with better captions. *Computer Science. https://cdn.openai.com/papers/dall-e-3.pdf*, 2(3):8, 2023.

Hongrui Chen, Holden Lee, and Jianfeng Lu. Improved analysis of score-based generative modeling: User-friendly bounds under minimal smoothness assumptions. In *International Conference on Machine Learning*, pp. 4735–4763, 2023.

Minshuo Chen, Song Mei, Jianqing Fan, and Mengdi Wang. An overview of diffusion models: Applications, guided generation, statistical rates and optimization. *arXiv preprint arXiv:2404.07771*, 2024.

Li Deng. The mnist database of handwritten digit images for machine learning research. *IEEE Signal Processing Magazine*, 29(6):141–142, 2012.

Prafulla Dhariwal and Alexander Nichol. Diffusion models beat gans on image synthesis. *Advances in Neural Information Processing Systems*, 34:8780–8794, 2021.

Tim Dockhorn, Arash Vahdat, and Karsten Kreis. Score-based generative modeling with critically-damped langevin diffusion. In *International Conference on Learning Representations*, 2021.

Patrick Esser, Sumith Kulal, Andreas Blattmann, Rahim Entezari, Jonas Müller, Harry Saini, Yam Levi, Dominik Lorenz, Axel Sauer, Frederic Boesel, et al. Scaling rectified flow transformers for high-resolution image synthesis. In *International Conference on Machine Learning*, 2024.

Ian Goodfellow, Jean Pouget-Abadie, Mehdi Mirza, Bing Xu, David Warde-Farley, Sherjil Ozair, Aaron Courville, and Yoshua Bengio. Generative adversarial nets. *Advances in neural information processing systems*, 27, 2014.

Arthur Gretton, Karsten M Borgwardt, Malte J Rasch, Bernhard Schölkopf, and Alexander Smola. A kernel two-sample test. *The Journal of Machine Learning Research*, 13(1):723–773, 2012. ISSN 1532-4435.

Hanzhong Guo, Cheng Lu, Fan Bao, Tianyu Pang, Shuicheng Yan, Chao Du, and Chongxuan Li. Gaussian mixture solvers for diffusion models. *Advances in Neural Information Processing Systems*, 36:25598–25626, 2023.

Ulrich G Haussmann and Etienne Pardoux. Time reversal of diffusions. *The Annals of Probability*, pp. 1188–1205, 1986.

Jonathan Ho, Ajay Jain, and Pieter Abbeel. Denoising diffusion probabilistic models. *Advances in Neural Information Processing Systems*, 33:6840–6851, 2020.

Aapo Hyvärinen and Peter Dayan. Estimation of non-normalized statistical models by score matching. *Journal of Machine Learning Research*, 6(4), 2005.

Tero Karras, Miika Aittala, Timo Aila, and Samuli Laine. Elucidating the design space of diffusion-based generative models. *Advances in neural information processing systems*, 35:26565–26577, 2022.

Ivan Kobyzev, Simon JD Prince, and Marcus A Brubaker. Normalizing flows: An introduction and review of current methods. *IEEE Transactions on Pattern Analysis and Machine Intelligence*, 43 (11):3964–3979, 2020.

Frederic Koehler, Alexander Heckett, and Andrej Risteski. Statistical efficiency of score matching: The view from isoperimetry. In *International Conference on Learning Representations*, 2023.

Gen Li, Yuting Wei, Yuxin Chen, and Yuejie Chi. Towards faster non-asymptotic convergence for diffusion-based generative models. *arXiv preprint arXiv:2306.09251*, 2023.

Gen Li, Yu Huang, Timofey Efimov, Yuting Wei, Yuejie Chi, and Yuxin Chen. Accelerating convergence of score-based diffusion models, provably. *arXiv preprint arXiv:2403.03852*, 2024.

Yuchen Liang, Peizhong Ju, Yingbin Liang, and Ness Shroff. Non-asymptotic Convergence of Discrete-time Diffusion Models: New Approach and Improved Rate, May 2024. arXiv preprint arXiv:2402.13901.

Ziwei Liu, Ping Luo, Xiaogang Wang, and Xiaoou Tang. Deep learning face attributes in the wild. In *International Conference on Computer Vision*, December 2015.

Cheng Lu, Kaiwen Zheng, Fan Bao, Jianfei Chen, Chongxuan Li, and Jun Zhu. Maximum likelihood training for score-based diffusion odes by high order denoising score matching. In *International Conference on Machine Learning*, pp. 14429–14460. PMLR, 2022.

Chenlin Meng, Yang Song, Wenzhe Li, and Stefano Ermon. Estimating high order gradients of the data distribution by denoising. *Advances in Neural Information Processing Systems*, 34: 25359–25369, 2021.

Alexander Quinn Nichol and Prafulla Dhariwal. Improved denoising diffusion probabilistic models. In *International Conference on Machine Learning*, pp. 8162–8171, 2021.

Zijing Ou, Mingtian Zhang, Andi Zhang, Tim Z. Xiao, Yingzhen Li, and David Barber. Improving probabilistic diffusion models with optimal diagonal covariance matching. In *International Conference on Learning Representations*, 2025.

Severi Rissanen, Markus Heinonen, and Arno Solin. Free hunch: Denoiser covariance estimation for diffusion models without extra costs. *arXiv preprint arXiv:2410.11149*, 2024.

Jascha Sohl-Dickstein, Eric Weiss, Niru Maheswaranathan, and Surya Ganguli. Deep unsupervised learning using nonequilibrium thermodynamics. In *International Conference on Machine Learning*, pp. 2256–2265, 2015.

Jiaming Song, Chenlin Meng, and Stefano Ermon. Denoising diffusion implicit models. In *International Conference on Learning Representations*, 2021a.

Yang Song, Sahaj Garg, Jiaxin Shi, and Stefano Ermon. Sliced score matching: A scalable approach to density and score estimation. In *Uncertainty in Artificial Intelligence*, pp. 574–584, 2020.

Yang Song, Conor Durkan, Iain Murray, and Stefano Ermon. Maximum likelihood training of score-based diffusion models. *Advances in Neural Information Processing Systems*, 34:1415–1428, 2021b.

Yang Song, Jascha Sohl-Dickstein, Diederik P Kingma, Abhishek Kumar, Stefano Ermon, and Ben Poole. Score-based generative modeling through stochastic differential equations. In *International Conference on Learning Representations*, 2021c.

Aad W Van der Vaart. *Asymptotic statistics*, volume 3. Cambridge university press, 2000.

Pascal Vincent. A connection between score matching and denoising autoencoders. *Neural computation*, 23(7):1661–1674, 2011.

Fangyikang Wang, Hubery Yin, Shaobin Zhuang, Huminhao Zhu, Yinan Li, Lei Qian, Chao Zhang, Hanbin Zhao, Hui Qian, and Chen Li. Efficiently access diffusion fisher: Within the outer product span space. *arXiv preprint arXiv:2505.23264*, 2025.

Joseph L Watson, David Juergens, Nathaniel R Bennett, Brian L Trippe, Jason Yim, Helen E Eisenach, Woody Ahern, Andrew J Borst, Robert J Ragotte, Lukas F Milles, et al. De novo design of protein structure and function with rfdiffusion. *Nature*, 620(7976):1089–1100, 2023.

Robert WM Wedderburn. Quasi-likelihood functions, generalized linear models, and the gauss—newton method. *Biometrika*, 61(3):439–447, 1974.

Ling Yang, Zhilong Zhang, Yang Song, Shenda Hong, Runsheng Xu, Yue Zhao, Wentao Zhang, Bin Cui, and Ming-Hsuan Yang. Diffusion models: A comprehensive survey of methods and applications. *ACM Computing Surveys*, 56(4):1–39, 2023.

Fisher Yu, Ari Seff, Yinda Zhang, Shuran Song, Thomas Funkhouser, and Jianxiong Xiao. LSUN: Construction of a Large-scale Image Dataset using Deep Learning with Humans in the Loop, 2016.

Kaiwen Zheng, Cheng Lu, Jianfei Chen, and Jun Zhu. Improved techniques for maximum likelihood estimation for diffusion odes. In *International Conference on Machine Learning*, pp. 42363–42389. PMLR, 2023.

A ALGORITHM

Algorithm 1: Likelihood Matching without time random sampling

---

Input: Dataset $\mathcal{D} = \{X_0^{(i)}\}_{i=1}^n \overset{\text{IID}}{\sim} q_0$, pre-determined time step set $\mathcal{T} = \{t_k\}_{k=1}^{N-1}$, learning rate η, batch size B

Output: Trained model: $\hat{s}_t(X_t; \phi)$ and $\hat{H}_t(X_t; \phi)$

1 // Training
2 **while** *not converge* **do**
3   **foreach** *batch* **do**
4   Get a mini-batch $\{X_0^{(i)}\}_{i=1}^B$ from $\mathcal{D}$ ($X_0^{(i)}$ is the i-th sample in the current batch);
5   **for** $k = 1, 2, \cdots, N$ **do**
6   Get perturbed data $\{X_t^{(i)}\}_{t=t_0}^{t_N}$
7   Calculate the transition term $\log \hat{p}_{t_{k-1}|t_k}(X_{t_{k-1}}^{(i)} | X_{t_k}^{(i)}; \phi)$
8   **end**
9   Calculate the batch loss $\mathcal{L}(\theta) = -B^{-1} \sum_{i=1}^B \sum_{k=1}^N \log \hat{p}_{t_{k-1}|t_k}(X_{t_{k-1}}^{(i)} | X_{t_k}^{(i)}; \phi)$
10   Update the parameter of s_t and H_t via stochastic gradient descent on:

$$\phi \leftarrow \phi - \eta \nabla_\phi \mathcal{L}(\phi)$$

11   **end**
12 **end**
13 Obtain the trained $\hat{s}_t(X_t; \phi)$ and $\hat{H}_t(X_t; \phi)$ // Also obtain the estimated parameter $\hat{\phi}$

Algorithm 2: Likelihood Matching with time random sampling

Input: $\mathcal{D} = \{X_0^{(i)}\}_{i=1}^n \overset{\text{IID}}{\sim} q_0$, learning rate η, batch size B, the number of chosen time points N

Output: Trained model: $\hat{s}_t(X_t; \phi)$ and $\hat{H}_t(X_t; \phi)$

1 // Training
2 **while** *not converge* **do**
3   **foreach** *batch* **do**
4   Get a mini-batch $\{X_0^{(i)}\}_{i=1}^B$ from $\mathcal{D}$ ($X_0^{(i)}$ is the i-th sample in the current batch);
5   Sample $(t_1^{(i)}, \cdots, t_{N-1}^{(i)}) \sim \text{Unif}\{(0, T)\}$ where $t_1^{(i)} < \cdots < t_{N-1}^{(i)}$ for $i = 1, \cdots, B$
6   **for** $k = 1, 2, \cdots, N$ **do**
7   Get perturbed data $\{X_t^{(i)}\}_{t=t_0}^{t_N}$
8   Calculate the transition term $\log \hat{p}_{t_{k-1}^{(i)}|t_k^{(i)}}(X_{t_{k-1}^{(i)}}^{(i)} | X_{t_k^{(i)}}^{(i)}; \phi)$
9   **end**
10   Calculate the batch loss $\mathcal{L}(\theta) = -B^{-1} \sum_{i=1}^B \sum_{k=1}^N \log \hat{p}_{t_{k-1}^{(i)}|t_k^{(i)}}(X_{t_{k-1}^{(i)}}^{(i)} | X_{t_k^{(i)}}^{(i)}; \phi)$
11   Update the parameter of s_t and H_t via stochastic gradient descent on:

$$\phi \leftarrow \phi - \eta \nabla_\phi \mathcal{L}(\phi)$$

12   **end**
13 **end**
14 Obtain the trained $\hat{s}_t(X_t; \phi)$ and $\hat{H}_t(X_t; \phi)$ // Also obtain the estimated parameter $\hat{\phi}$

B TECHNICAL RESULTS AND PROOFS

We first review the noise schedule proposed in Li et al. (2023). For sufficiently large constants $c_0, c_1 > 0$, define

$$
\begin{aligned}
e^{-\int_0^1 \beta_t \mathrm{d}t} &= \alpha_1 = \frac{1}{T^{c_0}}, \\
e^{-\int_{t-1}^t \beta_t \mathrm{d}t} &= \alpha_t = \frac{c_1 \log T}{T} \min\{(1+\alpha_1)(1+\frac{c_1 \log T}{T})^t, 1\}.
\end{aligned}
\tag{18}
$$

As established by Li et al. (2023), this specification ensures $\alpha_t \geq 1/2$ and $1 - \alpha_t \lesssim \log T/T$.

B.1 PROOF OF PROPOSITION 1

According to the definition of a time-reversal process in Haussmann & Pardoux (1986), when β_t of (1) is bounded and $\int_0^T \int_{\mathcal{O}} (\|q_t(x;\theta)\|^2 + d \cdot \beta_t \|\nabla q_t(x;\theta)\|^2) \mathrm{d}x \mathrm{d}t < \infty$, the time-reversal process of X_t exits, i.e., we have $Y_t \overset{d}{=} X_t$ and Y_t evolves from (2). Then the finite-dimensional distribution for the process Y_t is identically distributed as the associated distribution for process X_t. Therefore, we have

$$
q_{t_0:t_N}(x_{t_0}, x_{t_1}, \cdots, x_{t_N}; \theta) = p_{t_0:t_N}(x_{t_0}, x_{t_1}, \cdots, x_{t_N}; \theta),
\tag{19}
$$

for every $(x_{t_0}, x_{t_1}, \cdots, x_{t_N}; \theta) \in \mathbb{R}^{N+1} \times \Theta$. Thus, if we take the logarithm of both sides of the above equation, we will have

$$
\log q_{t_0}(X_{t_0}; \theta) + \sum_{k=1}^N \log q_{t_k|t_{k-1}}(X_{t_k}|X_{t_{k-1}}) = \log p_{t_N}(X_{t_N}; \theta) + \sum_{k=1}^N \log p_{t_{k-1}|t_k}(X_{t_{k-1}}|X_{t_k}; \theta).
\tag{20}
$$

Taking the expectation with respect to $(X_0, X_1, \cdots, X_T)$, we obtain (7) immediately.

B.2 PROOF OF PROPOSITION 2

By the definition of SDE (1), we have

$$
X_t|X_s \sim \mathcal{N}_d\left(m_{t|s} X_s, \sigma_{t|s}^2 I_d\right),
$$

where $m_{t|s} = \exp\{-\int_s^t \beta_t \mathrm{d}t/2\}$ and $\sigma_{t|s}^2 = 1 - \exp\{-\int_s^t \beta_t \mathrm{d}t\}$. Then we have

$$
\begin{aligned}
\nabla_{X_t} \log q_t(X_t; \theta) &= \frac{1}{q_t(X_t; \theta)} \nabla_{X_t} q_t(X_t; \theta) \\
&= \frac{1}{q_t(X_t; \theta)} \nabla_{X_t} \int q_{t|s}(X_t|X_s) q_s(X_s; \theta) \mathrm{d}X_s \\
&= \frac{1}{q_t(X_t; \theta)} \int \nabla_{X_t} q_{t|s}(X_t|X_s) q_s(X_s; \theta) \mathrm{d}X_s \\
&= \int \frac{q_{t|s}(X_t|X_s) q_s(X_s; \theta)}{q_t(X_t; \theta)} \nabla_{X_t} \log q_{t|s}(X_t|X_s) \mathrm{d}X_s \\
&= \int q_{s|t}(X_s|X_t; \theta) \frac{m_{t|s} X_s - X_t}{\sigma_{t|s}^2} \mathrm{d}X_s \\
&= \frac{m_{t|s} \mathbb{E}(X_s|X_t) - X_t}{\sigma_{t|s}^2}
\end{aligned}
\tag{21}
$$

which implies that

$$
\mu_{s|t} = \mathbb{E}(X_s|X_t) = \frac{X_t + \sigma_{t|s}^2 \nabla_{X_t} \log q_t(X_t)}{m_{t|s}}.
\tag{22}
$$

For the covariance, note that

$$
\Sigma_{s|t} = \mathbb{E}(X_s X_s^T | X_t) - \mathbb{E}(X_s|X_t) \mathbb{E}(X_s|X_t)^T.
$$

To derive the covariance, we need to compute the second gradient of $\log q_t(X_t; \theta)$. By taking the gradient of (21) with respect to X_t and using the same argument as above, we have

$$
\begin{aligned}
\nabla^2_{X_t} \log q_t(X_t; \theta) &= \int \frac{m_{t|s} X_s}{\sigma^2_{t|s}} \big\{ \nabla_{X_t} q_{s|t}(X_s | X_t; \theta) \big\}^T \mathrm{d}X_s - \frac{1}{\sigma^2_{t|s}} I_d \\
&= \int \frac{m_{t|s} X_s}{\sigma^2_{t|s}} q_{s|t}(X_s | X_t; \theta) \big\{ \nabla_{X_t} \log q_{s|t}(X_s | X_t; \theta) \big\}^T \mathrm{d}X_s - \frac{1}{\sigma^2_{t|s}} I_d \\
&= \int q_{s|t}(X_s | X_t; \theta) \frac{m_{t|s} X_s}{\sigma^2_{t|s}} \big\{ \nabla_{X_t} \log q_{t|s}(X_t | X_s) - \nabla_{X_t} \log q_t(X_t; \theta) \big\}^T \mathrm{d}X_s \\
&\quad - \frac{1}{\sigma^2_{t|s}} I_d \\
&= \int q_{s|t}(X_s | X_t; \theta) \frac{m_{t|s} X_s}{\sigma^2_{t|s}} \big\{ \nabla_{X_t} \log q_{t|s}(X_t | X_s) \big\}^T \mathrm{d}X_s \\
&\quad - \frac{m_{t|s} \mathbb{E}(X_s | X_t)}{\sigma^2_{t|s}} \big\{ \nabla_{X_t} \log q_t(X_t; \theta) \big\}^T - \frac{1}{\sigma^2_{t|s}} I_d \\
&= \int q_{s|t}(X_s | X_t; \theta) \frac{m_{t|s} X_s}{\sigma^2_{t|s}} \left\{ \frac{m_{t|s} X_s - X_t}{\sigma^2_{t|s}} \right\}^T \mathrm{d}X_s \\
&\quad - \frac{m_{t|s} \mathbb{E}(X_s | X_t)}{\sigma^2_{t|s}} \left\{ \frac{m_{t|s} \mathbb{E}(X_s | X_t) - X_t}{\sigma^2_{t|s}} \right\}^T - \frac{1}{\sigma^2_{t|s}} I_d \\
&= \left(\frac{m_{t|s}}{\sigma^2_{t|s}} \right)^2 \big\{ \mathbb{E}(X_s X_s^T | X_t) - \mathbb{E}(X_s | X_t) \mathbb{E}(X_s | X_t)^T \big\} - \frac{1}{\sigma^2_{t|s}} I_d.
\end{aligned}
$$

Hence, we conclude

$$
\Sigma_{s|t} = \frac{\sigma^4_{t,s}}{m^2_{t|s}} \nabla^2_{X_t} \log q_t(X_t; \theta) + \frac{\sigma^2_{t|s}}{m^2_{t|s}} I_d.
$$

This completes the proof.

B.3 PROOF OF THEOREM 1

From Pinsker's inequality, the first inequality is obvious. Thus, we focus on the second inequality. By data-processing inequality, we have

$$
\begin{aligned}
\mathrm{KL}(q_0 \| \tilde{p}_0) &\le \mathrm{KL}(q_{0:T} \| \tilde{p}_{0:T}) \\
&= \mathbb{E}_{X_{0:T} \sim q_{0:T}} \left[\log \left(\frac{q_{0:T}(X_0, X_1, \cdots, X_T)}{\tilde{p}_{0:T}(X_0, X_1, \cdots, X_T)} \right) \right] \\
&= \mathbb{E}_{X_{0:T} \sim q_{0:T}} \left[\log \left(\frac{q_T(X_T)}{\tilde{p}_T(X_T)} \right) + \sum_{t=1}^{T} \log \left(\frac{q_{t-1|t}(X_{t-1} | X_t)}{\tilde{p}_{t-1|t}(X_{t-1} | X_t)} \right) \right] \\
&= \underbrace{\mathrm{KL}(q_T \| \tilde{p}_T)}_{\mathcal{I}_1:\ \text{prior distribution error}} + \underbrace{\sum_{t=1}^{T} \mathbb{E}_{X_t \sim q_t} \big[\mathrm{KL}\big(q_{t-1|t}(\cdot | X_t) \| \tilde{p}_{t-1|t}(\cdot | X_t)\big) \big]}_{\mathcal{I}_2:\ \text{transition density ratio error}}
\end{aligned}
\tag{23}
$$

With the above decomposition, we now start to bound the two terms.

B.3.1 STEP 1: CONTROLLING THE PRIOR DISTRIBUTION ERROR

Lemma 1. *Under Assumptions 1, we have*

$$
\mathrm{KL}(q_T \| \tilde{p}_T) \le \frac{1}{2} d \bar{\alpha}_T^2 + \frac{1}{2} \bar{\alpha}_T M_2 \lesssim \frac{d}{T^{2c_2}} + \frac{1}{T^{c_2}}
\tag{24}
$$

for $T \ge 1$ and $c_2 \ge 1000$ is a large constant.

The proof of Lemma 1 can be found in Appendix B.5.1.

B.3.2 STEP 2: CONTROLLING THE TRANSITION DENSITY RATIO ERROR

We follow a similar argument in Li et al. (2023) to bound the second term. To begin with, we define the following true posterior mean and covariance mapping:

$$
\begin{aligned}
\mu^*_{t-1|t}(X_t) &= \frac{1}{\sqrt{\alpha_t}}(X_t + (1-\alpha_t)\nabla \log q_t(X_t)), \\
&:= \frac{1}{\sqrt{\alpha_t}}(X_t + (1-\alpha_t)s^*_t(X_t)), \\
\Sigma^*_{t-1|t}(X_t) &= \frac{1-\alpha_t}{\alpha_t}\{I_d + (1-\alpha_t)\nabla^2 \log q_t(X_t)\}, \\
&:= \frac{1-\alpha_t}{\alpha_t}\{I_d + (1-\alpha_t)H^*_t(X_t)\}.
\end{aligned}
\tag{25}
$$

and the estimated mapping as follows:

$$
\begin{aligned}
\hat{\mu}_{t-1|t}(X_t) &= \frac{1}{\sqrt{\alpha_t}}(X_t + (1-\alpha_t)\hat{s}_t(X_t)), \\
\hat{\Sigma}_{t-1|t}(X_t) &= \frac{1-\alpha_t}{\alpha_t}\{I_d + (1-\alpha_t)\hat{H}_t(X_t)\}.
\end{aligned}
\tag{26}
$$

It is clear that the transition density of $\tilde{Y}_{t-1}$ given $\tilde{Y}_t$ is

$$
\begin{aligned}
\tilde{p}_{t-1|t}(X_{t-1}|X_t) =& \left(2\pi\frac{1-\alpha_t}{\alpha_t}\right)^{-\frac{d}{2}}\left|I_d + (1-\alpha_t)\hat{H}_t(X_t)\right|^{-\frac{1}{2}} \\
& \cdot \exp\left\{-\frac{\alpha_t}{2(1-\alpha_t)}\left\|\left(I_d + (1-\alpha_t)\hat{H}_t(X_t)\right)^{-\frac{1}{2}}(X_{t-1} - \hat{\mu}_{t-1|t}(X_t))\right\|^2\right\}.
\end{aligned}
\tag{27}
$$

For any t, we introduce the following auxiliary sequences with the true score function and true Hessian function of the marginal density q_t as follows:

$$
H_{t-1} = \mu^*_{t-1|t}(H_t) + \Sigma^*_{t-1|t}(H_t)^{1/2}Z_t,
\tag{28}
$$

where $H_T \sim \mathcal{N}_d(0, I_d)$ and we define p^H_t and $p^H_{t-1|t}$ as the marginal and transition density of H_t and $H_{t-1}|H_t$. The transition density of H_{t-1} given H_t is given by

$$
\begin{aligned}
p^H_{t-1|t}(X_{t-1}|X_t) =& \left(2\pi\frac{1-\alpha_t}{\alpha_t}\right)^{-\frac{d}{2}}|I_d + (1-\alpha_t)H^*_t(X_t)|^{-\frac{1}{2}} \\
& \cdot \exp\left\{-\frac{\alpha_t}{2(1-\alpha_t)}\left\|(I_d + (1-\alpha_t)H^*_t(X_t))^{-\frac{1}{2}}(X_{t-1} - \mu^*_{t-1|t}(X_t))\right\|^2\right\}.
\end{aligned}
\tag{29}
$$

Hence, the term $\mathcal{I}_2$ can be bounded as follows:

$$
\begin{aligned}
\mathcal{I}_2 =& \sum_{t=1}^{T}\mathbb{E}_{X_t\sim q_t}\left[\mathrm{KL}\big(q_{t-1|t}(\cdot|X_t)\|\tilde{p}_{t-1|t}(\cdot|X_t)\big)\right] \\
=& \underbrace{\sum_{t=1}^{T}\mathbb{E}_{X_t\sim q_t}\left\{\mathbb{E}_{X_{t-1}\sim q_{t-1|t}}\left[\log\frac{q_{t-1|t}(X_{t-1}|X_t)}{p^H_{t-1|t}(X_{t-1}|X_t)}\right]\right\}}_{\mathcal{I}_3:\text{ reverse step error}} \\
& + \underbrace{\sum_{t=1}^{T}\mathbb{E}_{X_t\sim q_t}\left\{\mathbb{E}_{X_{t-1}\sim q_{t-1|t}}\left[\log\frac{p^H_{t-1|t}(X_{t-1}|X_t)}{\tilde{p}_{t-1|t}(X_{t-1}|X_t)}\right]\right\}}_{\mathcal{I}_4:\text{ estimation error}}
\end{aligned}
\tag{30}
$$

17

To control the term $\mathcal{I}_3$, we introduce the following set in Li et al. (2023) :

$$\mathcal{E} = \left\{ (X_{t-1}, X_t) : -\log q_t(X_t) \lesssim d \log T, \|X_{t-1} - X_t/\sqrt{\alpha_t}\|^2 \lesssim \sqrt{d(1-\alpha_t)\log T} \right\}. \quad (31)$$

Turning to $q_{t-1|t}(X_{t-1}|X_t)$ over the set $\mathcal{E}$, we have the lemma as below:

Lemma 2. *There exists some large enough numerical constant $c_s > 0$ such that: for any $(X_{t-1}, X_t) \in \mathcal{E}$, we have*

$$
\begin{aligned}
& q_{t-1|t}(X_{t-1}|X_t) \\
&= \left(2\pi \frac{1-\alpha_t}{\alpha_t}\right)^{-\frac{d}{2}} |I_d + (1-\alpha_t)H_t^*(X_t)|^{-\frac{1}{2}} \\
&\quad \cdot \exp\left\{ -\frac{\alpha_t}{2(1-\alpha_t)} \left\| (I_d + (1-\alpha_t)H_t^*(X_t))^{-\frac{1}{2}} (X_{t-1} - \mu_{t-1|t}^*(X_t)) \right\|^2 + \varepsilon_t(X_{t-1}, X_t) \right\},
\end{aligned}
\quad (32)
$$

where the residual term $\varepsilon_t(X_{t-1}, X_t)$ satisfies

$$|\varepsilon_t(X_{t-1}, X_t)| \leq c_s \frac{d^3 \log^{4.5} T}{T^{3/2}}. \quad (33)$$

The proof of Lemma 2 is provided in Appendix B.5.2.

We can observe that under the set $\mathcal{E}$, the transition density $p_{t-1|t}^H(X_{t-1}|X_t)$ is nearly equal to the transition density $p_{H_{t-1}|H_t}(X_{t-1}|X_t)$ defined in Li et al. (2024). With the proof of Lemma 11 in Li et al. (2024) and using (55) and (56), we know that

$$(I_d + (1-\alpha_t)H_t^*(X_t))^{-1} = (I_d + \frac{1}{2}(1-\alpha_t)H_t^*(X_t))^{-2} + A, \quad (34)$$

where

$$\|A\| \lesssim \frac{d^2 \log^4 T}{T^2}. \quad (35)$$

Therefore, we have

$$\frac{p_{t-1|t}^H(X_{t-1}|X_t)}{p_{H_{t-1}|H_t}(X_{t-1}|X_t)} = 1 + O\left(\frac{d^3 \log^5 T}{T^2}\right). \quad (36)$$

Then, we introduce some useful lemmas established by Li et al. (2024).

Lemma 3 (Lemma 11 in Li et al. (2024)). *For every $(X_t, X_{t-1}) \in \mathcal{E}$, we have*

$$
\begin{aligned}
& p_{H_{t-1}|H_t}(X_{t-1}|X_t) \\
&\propto \exp\left\{ -\frac{\alpha_t}{2(1-\alpha_t)} \left\| (I + (1-\alpha_t)H_t^*(X_t))^{-1} \left(X_{t-1} - \mu_{t-1|t}^*(X_t)\right) \right\|^2 + O\left(\frac{d^3 \log^5 T}{T^2}\right) \right\}.
\end{aligned}
\quad (37)
$$

Lemma 4 (Lemma 13 in Li et al. (2024)). *For all $(X_t, X_{t-1}) \in \mathbb{R}^d \times \mathbb{R}^d$, we have*

$$\log \frac{q_{t|t-1}(X_{t-1}|X_t)}{p_{H_{t-1}|H_t}(X_{t-1}|X_t)} \leq T^{c_0+2c_R+2} \left\{ \|X_{t-1} - X_t/\sqrt{\alpha_t}\|_2^2 + \|X_t\|_2^2 + 1 \right\},$$

where c_0 is defined in (18) and c_R is defined in Lemma 3 in Li et al. (2024).

By (36), we know that Lemmas 3 and 4 can be applied in our cases. And with Lemma 2, one can repeat the arguments in the proof of Lemma 14 in Li et al. (2024), and get the same results as follows:

$$\mathcal{I}_3 = \sum_{t=1}^{T} \mathbb{E}_{X_t \sim q_t} \left[\mathrm{KL}\left(q_{t-1|t}(\cdot|X_t) \| p_{t-1|t}^H(\cdot|X_t) \right) \right] \lesssim \sum_{t=1}^{T} \frac{d^6 \log^9 T}{T^3} \asymp \frac{d^6 \log^9 T}{T^2}. \quad (38)$$

To control the term $\mathcal{I}_4$, we introduce the following lemma.

Lemma 5. *Under Assumptions 2, 3 and 4, we have*

$$\sum_{t=1}^{T} \mathbb{E}_{X_t \sim q_t} \left\{ \mathbb{E}_{X_{t-1} \sim q_{t-1|t}} \left[\log \frac{p_{t-1|t}^H(X_{t-1}|X_t)}{\tilde{p}_{t-1|t}(X_{t-1}|X_t)} \right] \right\} \lesssim \log T \varepsilon_s^2 + \frac{\log^2 T}{T} \varepsilon_H^2. \tag{39}$$

The proof of Lemma 5 can be found in Appendix B.5.2.

Combining (38) and Lemma 5 yields

$$\mathcal{I}_2 \lesssim \frac{d^6 \log^9 T}{T^2} + \log T \varepsilon_s^2 + \frac{\log^2 T}{T} \varepsilon_H^2. \tag{40}$$

Therefore, from Lemma 1 and (40), we arrive at

$$\begin{aligned}
\mathrm{KL}(q_0 || \tilde{p}_0) &\lesssim \frac{d}{T^{2c_2}} + \frac{1}{T^{c_2}} + \frac{d^6 \log^9 T}{T^2} + \log T \varepsilon_s^2 + \frac{\log^2 T}{T} \varepsilon_H^2 \\
&\asymp \frac{d^6 \log^9 T}{T^2} + \log T \varepsilon_s^2 + \frac{\log^2 T}{T} \varepsilon_H^2
\end{aligned} \tag{41}$$

thereby concluding the proof of Theorem 1.

B.4 PROOF OF THEOREM 2

Denoted by

$$\begin{aligned}
\tilde{M}_{n,T}(\theta) &:= \frac{1}{n} \sum_{i=1}^{n} \log q_{0:T}(X_0^{(i)}, X_1^{(i)}, ..., X_T^{(i)}; \theta), \\
\hat{M}_{n,T}(\theta) &:= \frac{1}{n} \sum_{i=1}^{n} \sum_{t=1}^{T} \log \hat{p}_{t-1|t}(X_{t-1}^{(i)} | X_t^{(i)}; \theta) + \frac{1}{n} \sum_{i=1}^{n} \log \tilde{p}_T(X_T^{(i)}), \\
M_T(\theta) &:= \mathbb{E}_{X_{0:T} \sim q_{0:T}} \left[\log q_{0:T}(X_0, ..., X_T; \theta) \right],
\end{aligned} \tag{42}$$

where $\tilde{p}_T(\cdot)$ denotes the density for d-dimensional standard normal distribution, $\hat{\theta}_{n,T} := \arg\min_\theta \mathcal{J}_{n,N}(\theta) = \arg\max_\theta \hat{M}_{n,T}(\theta)$, and $\tilde{\theta}_{n,T} := \arg\max_\theta \tilde{M}_{n,T}(\theta)$.

We assume that the following regularity conditions are satisfied

(1) The forward sampling procedure employs an equidistant grid with step size Δ, which maintains an inverse proportionality relationship with the terminal time T.

(2) $\sup_\theta \left| \tilde{M}_{n,T}(\theta) - M_T(\theta) \right| \xrightarrow{p} 0$, as $n, T \to \infty$.

(3) For any $\epsilon > 0$, there exits a constant η, such that

$$\sup_{|\theta - \theta^*| \geq \epsilon} M_T(\theta) < M_T(\theta^*) - \eta, \quad \text{for} \quad \forall n, T.$$

(4) We suppose a uniform logarithmic approximation as follows:

$$\sup_{\theta, x_0, \cdots, x_T} \left| \log \left(\frac{q_{0:T-1|T}(x_0, x_1, ..., x_{T-1} | x_T; \theta)}{\hat{p}_{0:T-1|T}(x_0, x_1, ..., x_{T-1} | x_T; \theta)} \right) \right| \leq \epsilon_2(T),$$

where $\lim_{T \to \infty} \epsilon_2(T) = 0$.

The first two conditions are basically modified From Theorem 5.7 of Van der Vaart (2000) to ensure the consistency of true maximum likelihood estimation obtained from $\tilde{M}_{n,T}(\theta)$, i.e., $\tilde{\theta}_{n,T}$. And the third and fourth can be intuitively interpreted as the approximated likelihood behaves well, namely, the error can be uniformly bounded.

We observe that

$$\begin{aligned}
\tilde{M}_{n,T}(\tilde{\theta}_{n,T}) &\geq \tilde{M}_{n,T}(\theta^*) \\
&= M_T(\theta^*) + \tilde{M}_{n,T}(\theta^*) - M_T(\theta^*) \\
&\geq M_T(\theta^*) - \sup_\theta \left| \tilde{M}_{n,T}(\theta) - M_T(\theta) \right|.
\end{aligned} \tag{43}$$

19

Thus, combined with (43), we obtain

$$
\begin{aligned}
M_T(\theta^*) - M_T(\tilde{\theta}_{n,T}) &\leq \tilde{M}_{n,T}(\tilde{\theta}_{n,T}) - M_T(\tilde{\theta}_{n,T}) + \sup_\theta \left| \tilde{M}_{n,T}(\theta) - M_T(\theta) \right| \\
&\leq 2 \sup_\theta \left| \tilde{M}_{n,T}(\theta) - M_T(\theta) \right|.
\end{aligned}
\tag{44}
$$

Similarly to (43), we have the following results for $\hat{\theta}_{n,T}$, i.e.,

$$
\begin{aligned}
\hat{M}_{n,T}(\hat{\theta}_{n,T}) &\geq \hat{M}_{n,T}(\theta^*) \\
&= M_T(\theta^*) + \hat{M}_{n,T}(\theta^*) - M_T(\theta^*) \\
&\geq M_T(\theta^*) - \sup_\theta \left| \hat{M}_{n,T}(\theta) - M_T(\theta) \right|,
\end{aligned}
\tag{45}
$$

and

$$
\begin{aligned}
M_T(\theta^*) - M_T(\hat{\theta}_{n,T}) &\leq \hat{M}_{n,T}(\hat{\theta}_{n,T}) - M_T(\hat{\theta}_{n,T}) + \sup_\theta \left| \hat{M}_{n,T}(\theta) - M_T(\theta) \right| \\
&\leq 2 \sup_\theta \left| \hat{M}_{n,T}(\theta) - M_T(\theta) \right|,
\end{aligned}
\tag{46}
$$

by plugging (45) into the first inequality.

Therefore, we are motivated to investigate how large $\sup_\theta \left| \hat{M}_{n,T}(\theta) - M_T(\theta) \right|$ will be. We notice that

$$
\sup_\theta \left| \hat{M}_{n,T}(\theta) - M_T(\theta) \right| \leq \sup_\theta \left| \tilde{M}_{n,T}(\theta) - M_T(\theta) \right| + \sup_\theta \left| \tilde{M}_{n,T}(\theta) - \hat{M}_{n,T}(\theta) \right|.
\tag{47}
$$

Since $\sup_\theta |\tilde{M}_{n,T}(\theta) - M_T(\theta)|$ is an $o_p(1)$ term, we only need to compute $\sup_\theta |\tilde{M}_{n,T}(\theta) - \hat{M}_{n,T}(\theta)|$. Notice that

$$
\begin{aligned}
&\tilde{M}_{n,T}(\theta) - \hat{M}_{n,T}(\theta) \\
&= \frac{1}{n} \sum_{i=1}^n \log \left(\frac{q_{0:T-1|T}(X_0^{(i)}, X_1^{(i)}, ..., X_{T-1}^{(i)} | X_T^{(i)}; \theta)}{\hat{p}_{0:T-1|T}(X_0^{(i)}, X_1^{(i)}, ..., X_{T-1}^{(i)} | X_T^{(i)}; \theta)} \right) + \frac{1}{n} \sum_{i=1}^n \log \left(\frac{q_T(X_T^{(i)})}{\tilde{p}_T(X_T^{(i)})} \right),
\end{aligned}
$$

and from Condition (3), we have

$$
\sup_{\theta, x_0, \cdots, x_T} \left| \log \left(\frac{q_{0:T-1|T}(x_0, x_1, ..., x_{T-1} | x_T; \theta)}{\hat{p}_{0:T-1|T}(x_0, x_1, ..., x_{T-1} | x_T; \theta)} \right) \right| \leq \epsilon_2(T).
\tag{48}
$$

Also, according to Lemma 1 and the law of large numbers, we have

$$
\frac{1}{n} \sum_{i=1}^n \log \left(\frac{q_T(X_T^{(i)})}{\tilde{p}_T(X_T^{(i)})} \right) \xrightarrow{p} \mathrm{KL}(q_T || \tilde{p}_T),
\tag{49}
$$

which implies

$$
\frac{1}{n} \sum_{i=1}^n \log \left(\frac{q_T(X_T^{(i)})}{\tilde{p}_T(X_T^{(i)})} \right) = \epsilon_3(n, T),
$$

where $\epsilon_3(n, T) \xrightarrow{p} 0$, as n and T tend to ∞. Thus, we can decompose (46) as

$$
\begin{aligned}
M_T(\theta^*) - M_T(\hat{\theta}_{n,T}) &\leq 2 \left(\sup_\theta \left| \tilde{M}_{n,T}(\theta) - M_T(\theta) \right| + \sup_\theta \left| \tilde{M}_{n,T}(\theta) - \hat{M}_{n,T}(\theta) \right| \right) \\
&\leq 2 \sup_\theta \left| \tilde{M}_{n,T}(\theta) - M_T(\theta) \right| + 2\epsilon_2(T) + 2\epsilon_3(n, T).
\end{aligned}
$$

We observe that $\{\theta : |\theta - \theta^*| \geq \epsilon\} \subset \{\theta : M_T(\theta) < M_T(\theta^*) - \eta\}$. Thus, when n, T is sufficiently large, such that $\sup_\theta |\tilde{M}_{n,T}(\theta) - M_T(\theta)| + \epsilon_2(T) + \epsilon_3(n, T) < \eta/2$, we obtain $|\hat{\theta}_{n,T} - \theta^*| < \epsilon$, which leads to

$$
\hat{\theta}_{n,T} \xrightarrow{p} \theta^*, \quad \text{as} \quad n, T \to \infty.
\tag{50}
$$

B.5 PROOF OF AUXILIARY LEMMAS

B.5.1 PROOF OF LEMMA 1

Note that $\tilde{p}_T(X_T)$ is $\mathcal{N}_d(0, I_d)$ and $q_{t|0}(x|y) = \mathcal{N}(x; m_t y, \sigma_t^2 I_d)$, where $m_t = \sqrt{\bar{\alpha}_t}$ and $\sigma_t^2 = 1 - \bar{\alpha}_t$, we obtain

$$\mathrm{KL}(q_{t|0}(\cdot|y)||\mathcal{N}_d(0, I_d)) = \frac{1}{2}\Big(-d(1 - \sigma_t^2) - d\log \sigma_t^2 + m_t^2\|y\|^2\Big).$$

By the convexity of the KL divergence, we have

$$
\begin{aligned}
\mathrm{KL}(q_T||\mathcal{N}_d(0, I_d)) &= \mathrm{KL}\Big(\int_{\mathbb{R}^d} q_{T|0}(x|y)\mathrm{d}Q_0(y)||\mathcal{N}_d(0, I_d)\Big) \\
&\leq \int_{\mathbb{R}^d} \mathrm{KL}(q_{T|0}(\cdot|y)||\mathcal{N}_d(0, I_d))\mathrm{d}Q_0(y) \\
&= \frac{1}{2}\int_{\mathbb{R}^d} \Big(-d(1 - \sigma_T^2) - d\log \sigma_T^2 + m_T^2\|y\|^2\Big)\mathrm{d}Q_0(y) \\
&= \frac{1}{2}\Big(-d(1 - \sigma_T^2) - d\log \sigma_T^2 + m_T^2\mathbb{E}_{X\sim q_0}\|X\|^2\Big) \\
&\leq \frac{1}{2}(-d\bar{\alpha}_T - d\log(1 - \bar{\alpha}_T) + \bar{\alpha}_T M_2).
\end{aligned}
\tag{51}
$$

Since $\log(1 + x) > x - x^2$ when $x > -0.68$ and $\bar{\alpha}_T < 0.68$ when $T \geq 1$, we obtain

$$-\log(1 - \bar{\alpha}_T) < \bar{\alpha}_T + \bar{\alpha}_T^2.$$

Thus

$$\mathrm{KL}(q_T||\tilde{p}_T) \leq \frac{1}{2}d\bar{\alpha}_T^2 + \frac{1}{2}\bar{\alpha}_T M_2 \lesssim \frac{d}{T^{2c_2}} + \frac{1}{T^{c_2}}, \tag{52}$$

where $c_2 \geq 1000$ and the last inequality holds by the properties of the noise schedule in Li et al. (2023).

B.5.2 PROOF OF LEMMA 2

Lemma 12 in Li et al. (2023) shows that the transition density of X_{t-1} given X_t can be expressed as

$$q_{t-1|t}(X_{t-1}|X_t) = f_1(X_t)\exp\{-f_2(X_{t-1}, X_t) + \varepsilon_{t,1}(X_{t-1}, X_t)\} \tag{53}$$

for some function $f_1(\cdot)$, where

$$
\begin{aligned}
&f_2(X_{t-1}, X_t) \\
&= \frac{\alpha_t}{2(1 - \alpha_t)}\left\{\Big(X_{t-1} - \mu_{t-1|t}^*(X_t)\Big)^T (I_d - (1 - \alpha_t)H_t^*(X_t))\Big(X_{t-1} - \mu_{t-1|t}^*(X_t)\Big)\right\}
\end{aligned}
\tag{54}
$$

and

$$|\varepsilon_{t,1}(X_{t-1}, X_t)| \lesssim \frac{d^3\log^{4.5} T}{T^{3/2}}.$$

Note that the formulation of the covariance matrix $I_d - (1 - \alpha_t)H_t^*(X_t)$ still differs from $(I_d + (1 - \alpha_t)\hat{H}_t(X_t))^{-1}$. Following the same procedure in Li et al. (2023), we can show that

$$(I_d + (1 - \alpha_t)H_t^*(X_t))^{-1} = I_d - (1 - \alpha_t)H_t^*(X_t) + A, \tag{55}$$

where A is a matrix obeying

$$\|A\| \lesssim \frac{d^2\log^4 T}{T^2}. \tag{56}$$

Combining the above, we arrive at

$$q_{t-1|t}(X_{t-1}|X_t) = f_3(X_t)\exp\{-f_4(X_{t-1}, X_t) + \varepsilon_{t,2}(X_{t-1}, X_t)\} \tag{57}$$

for some function $f_3(\cdot)$, where

$$
\begin{aligned}
&f_4(X_{t-1}, X_t) \\
&= \frac{\alpha_t}{2(1 - \alpha_t)}\left\{\Big(X_{t-1} - \mu_{t-1|t}^*(X_t)\Big)^T (I_d - (1 - \alpha_t)H_t^*(X_t))^{-1}\Big(X_{t-1} - \mu_{t-1|t}^*(X_t)\Big)\right\}
\end{aligned}
\tag{58}
$$

and

$$|\varepsilon_{t,2}(X_{t-1}, X_t)| \lesssim \frac{d^3 \log^{4.5} T}{T^{3/2}}.$$

Repeating Step 3 in the proof of Lemma 8 in Li et al. (2023), it yields that

$$f_3(X_t) = \left(1 + O\left(\frac{d^3 \log^{4.5} T}{T^{3/2}}\right)\right)\left(2\pi \frac{1-\alpha_t}{\alpha_t}\right)^{-\frac{d}{2}} |I_d + (1-\alpha_t)H_t^*(X_t)|^{-\frac{1}{2}}.$$

This completes the proof.

B.5.3   PROOF OF LEMMA 5

Considering the approach in Liang et al. (2024), we directly calculate the density ratio between two Gaussian distributions with the different mean and different covariance. We have

$$\log \frac{p_{t-1|t}^H(X_{t-1}|X_t)}{\tilde{p}_{t-1|t}(X_{t-1}|X_t)}$$

$$=\frac{1}{2}\log\left(\frac{\det\left(I_d + (1-\alpha_t)\hat{H}_t(X_t)\right)}{\det(I_d + (1-\alpha_t)H_t^*(X_t))}\right) + \frac{\alpha_t}{2(1-\alpha_t)}(X_{t-1} - \hat{\mu}_{t-1|t}(X_t))^T$$

$$\cdot \left\{(I_d + (1-\alpha_t)\hat{H}_t(X_t))^{-1} - (I_d + (1-\alpha_t)H_t^*(X_t))^{-1}\right\}(X_{t-1} - \hat{\mu}_{t-1|t}(X_t))$$

$$+ \frac{\alpha_t}{2(1-\alpha_t)}(X_{t-1} - \hat{\mu}_{t-1|t}(X_t))^T(I_d + (1-\alpha_t)H_t^*(X_t))^{-1}(X_{t-1} - \hat{\mu}_{t-1|t}(X_t))$$

$$- \frac{\alpha_t}{2(1-\alpha_t)}(X_{t-1} - \mu_{t-1|t}^*(X_t))^T(I_d + (1-\alpha_t)H_t^*(X_t))^{-1}(X_{t-1} - \mu_{t-1|t}^*(X_t))$$

$$=\frac{1}{2}\log\left(\frac{\det\left(I_d + (1-\alpha_t)\hat{H}_t(X_t)\right)}{\det(I_d + (1-\alpha_t)H_t^*(X_t))}\right) + \frac{\alpha_t}{2(1-\alpha_t)}(\mu_{t-1|t}^*(X_t) - \hat{\mu}_{t-1|t}(X_t))^T$$

$$\cdot (I_d + (1-\alpha_t)H_t^*(X_t))^{-1}(\mu_{t-1|t}^*(X_t) - \hat{\mu}_{t-1|t}(X_t))$$

$$+ \frac{\alpha_t}{2(1-\alpha_t)}(X_{t-1} - \mu_{t-1|t}^*(X_t))^T\left\{(I_d + (1-\alpha_t)\hat{H}_t(X_t))^{-1} - (I_d + (1-\alpha_t)H_t^*(X_t))^{-1}\right\}$$

$$\cdot (X_{t-1} - \mu_{t-1|t}^*(X_t))$$

$$+ \frac{\alpha_t}{2(1-\alpha_t)}(X_{t-1} - \mu_{t-1|t}^*(X_t))^T\left\{(I_d + (1-\alpha_t)\hat{H}_t(X_t))^{-1} - (I_d + (1-\alpha_t)H_t^*(X_t))^{-1}\right\}$$

$$\cdot (\hat{\mu}_{t-1|t}^*(X_t) - \hat{\mu}_{t-1|t}(X_t))$$

$$+ \frac{\alpha_t}{2(1-\alpha_t)}(\hat{\mu}_{t-1|t}^*(X_t) - \hat{\mu}_{t-1|t}(X_t))^T\left\{(I_d + (1-\alpha_t)\hat{H}_t(X_t))^{-1}\right.$$

$$\left. - (I_d + (1-\alpha_t)H_t^*(X_t))^{-1}\right\} \cdot (X_{t-1} - \mu_{t-1|t}^*(X_t)).$$

$$(59)$$

For the last two terms in (59), we can observe that under the expectation w.r.t $X_{t-1} \sim q_{t-1|t}$, they are both zero. Thus, by a little algebra, we have

$$\mathbb{E}_{X_{t-1} \sim q_{t-1|t}} \log \frac{p_{t-1|t}^H(X_{t-1}|X_t)}{\tilde{p}_{t-1|t}(X_{t-1}|X_t)}$$

$$=\frac{1}{2}\log\left(\frac{\det\left(I_d + (1-\alpha_t)\hat{H}_t(X_t)\right)}{\det(I_d + (1-\alpha_t)H_t^*(X_t))}\right)$$

$$+ \frac{\alpha_t}{2(1-\alpha_t)}(\mu_{t-1|t}^*(X_t) - \hat{\mu}_{t-1|t}(X_t))^T(I_d + (1-\alpha_t)H_t^*(X_t))^{-1}(\mu_{t-1|t}^*(X_t) - \hat{\mu}_{t-1|t}(X_t))$$

$$+ \frac{1}{2}\mathbb{E}_{X_{t-1} \sim q_{t-1|t}} \operatorname{tr}\left[(I_d + (1-\alpha_t)\hat{H}_t(X_t))^{-1}(I_d + (1-\alpha_t)H_t^*(X_t)) - d\right].$$

$$(60)$$

Considering the second term in (60) and from Assumption 4, we obtain that

$$
\frac{\alpha_t}{2(1-\alpha_t)}\mathbb{E}_{X_t\sim q_t}\Big[(\mu^*_{t-1|t}(X_t)-\hat{\mu}_{t-1|t}(X_t))^T(I_d+(1-\alpha_t)H^*_t(X_t))^{-1}
$$
$$
\cdot(\mu^*_{t-1|t}(X_t)-\hat{\mu}_{t-1|t}(X_t))\Big]
$$
$$
=\frac{1-\alpha_t}{2}\mathbb{E}_{X_t\sim q_t}\Big[(s^*_t(X_t)-\hat{s}_t(X_t))^T(I_d+(1-\alpha_t)H^*_t(X_t))^{-1}(s^*_t(X_t)-\hat{s}_t(X_t))\Big]
$$
$$
\leq\frac{1-\alpha_t}{2}\mathbb{E}_{X_t\sim q_t}\Big[\|s^*_t(X_t)-\hat{s}_t(X_t)\|^2\big\|(I_d+(1-\alpha_t)H^*_t(X_t))^{-1}\big\|\Big]
$$
$$
\leq\frac{1-\alpha_t}{2(1+\varepsilon_0)}\mathbb{E}_{X_t\sim q_t}\|s^*_t(X_t)-\hat{s}_t(X_t)\|^2
$$
$$
\lesssim\frac{1-\alpha_t}{2}\mathbb{E}_{X_t\sim q_t}\|s^*_t(X_t)-\hat{s}_t(X_t)\|^2. \tag{61}
$$

For the first term in (60), the term $1-\alpha_t$ is small enough when t is large, thus we can use Taylor expansion to show that

$$
\mathbb{E}_{X_t\sim q_t}\log(\det(I_d+(1-\alpha_t)H^*_t(X_t)))
$$
$$
=\mathbb{E}_{X_t\sim q_t}\log\Big(1+(1-\alpha_t)\operatorname{tr}(H^*_t(X_t))+\frac{(1-\alpha_t)^2}{2}\operatorname{tr}(H^*_t(X_t))^2
$$
$$
-\frac{(1-\alpha_t)^2}{2}\operatorname{tr}\big(H^*_t(X_t)^2\big)+O((1-\alpha_t)^3)\Big)
$$
$$
=\mathbb{E}_{X_t\sim q_t}\Big[(1-\alpha_t)\operatorname{tr}(H^*_t(X_t))-\frac{(1-\alpha_t)^2}{2}\operatorname{tr}\big(H^*_t(X_t)^2\big)\Big]+O((1-\alpha_t)^3). \tag{62}
$$

Thus, by the same argument, we get

$$
\frac{1}{2}\mathbb{E}_{X_t\sim q_t}\log\left(\frac{\det\Big(I_d+(1-\alpha_t)\hat{H}_t(X_t)\Big)}{\det(I_d+(1-\alpha_t)H^*_t(X_t))}\right)
$$
$$
=\frac{1}{2}\mathbb{E}_{X_t\sim q_t}\Big[(1-\alpha_t)\operatorname{tr}\Big(\hat{H}_t(X_t)-H^*_t(X_t)\Big)-\frac{(1-\alpha_t)^2}{2}\operatorname{tr}\Big(\hat{H}_t(X_t)^2-H^*_t(X_t)^2\Big)\Big]
$$
$$
+O((1-\alpha_t)^3). \tag{63}
$$

For the third term in (60), we have

$$
\frac{1}{2}\mathbb{E}_{X_{t-1}\sim q_{t-1|t}}\operatorname{tr}\Big[(I_d+(1-\alpha_t)\hat{H}_t(X_t))^{-1}(I_d+(1-\alpha_t)H^*_t(X_t))-d\Big]
$$
$$
=\frac{1}{2}\mathbb{E}_{X_{t-1}\sim q_{t-1|t}}\operatorname{tr}\Big[(I_d-(1-\alpha_t)\hat{H}_t(X_t)+(1-\alpha_t)^2\hat{H}_t(X_t)^2+O((1-\alpha_t)^3))
$$
$$
\cdot(I_d+(1-\alpha_t)H^*_t(X_t))-d]
$$
$$
=\frac{1}{2}\mathbb{E}_{X_{t-1}\sim q_{t-1|t}}\operatorname{tr}\Big[(1-\alpha_t)\operatorname{tr}(H^*_t(X_t))-(1-\alpha_t)\operatorname{tr}\Big(\hat{H}_t(X_t)\Big)+(1-\alpha_t)^2\operatorname{tr}\Big(\hat{H}_t(X_t)^2\Big)\Big]
$$
$$
+O((1-\alpha_t)^2). \tag{64}
$$

23

Combining (61), (63) and (64), we arrive at

$$
\mathbb{E}_{X_t \sim q_t} \left\{ \mathbb{E}_{X_{t-1} \sim q_{t-1|t}} \log \frac{p_{t-1|t}^H(X_{t-1}|X_t)}{\tilde{p}_{t-1|t}(X_{t-1}|X_t)} \right\}
$$

$$
\lesssim \frac{(1-\alpha_t)^2}{2\alpha_t} \mathbb{E}_{X_t \sim q_t} \|s_t^*(X_t) - \hat{s}_t(X_t)\|^2
$$

$$
+ \frac{(1-\alpha_t)^2}{2} \mathbb{E}_{X_t \sim q_t} \left[\operatorname{tr}\left(\hat{H}_t(X_t)^2\right) + \operatorname{tr}\left(H_t^*(X_t)^2\right) - 2\operatorname{tr}\left(\hat{H}_t(X_t)H_t^*(X_t)\right) \right] + O((1-\alpha_t)^2)
$$

$$
= \frac{1-\alpha_t}{2} \mathbb{E}_{X_t \sim q_t} \|s_t^*(X) - \hat{s}_t(X)\|^2 + \frac{(1-\alpha_t)^2}{2} \mathbb{E}_{X_t \sim q_t} \operatorname{tr}\left((\hat{H}_t(X_t) - H_t^*(X_t))^2\right)
$$

$$
+ O((1-\alpha_t)^2)
$$

$$
= \frac{1-\alpha_t}{2} \mathbb{E}_{X_t \sim q_t} \|s_t^*(X) - \hat{s}_t(X)\|^2 + \frac{(1-\alpha_t)^2}{2} \mathbb{E}_{X_t \sim q_t} \left\|\hat{H}_t(X_t) - H_t^*(X_t)\right\|_F^2
$$

$$
+ O((1-\alpha_t)^2). \tag{65}
$$

Consequently, we can demonstrate that

$$
\sum_{t=1}^T \mathbb{E}_{X_t \sim q_t} \left\{ \mathbb{E}_{X_{t-1} \sim q_{t-1|t}} \log \frac{p_{t-1|t}^H(X_{t-1}|X_t)}{\tilde{p}_{t-1|t}(X_{t-1}|X_t)} \right\} \lesssim \frac{1-\alpha_t}{2} T\varepsilon_s^2 + \frac{(1-\alpha_t)^2}{2} T\varepsilon_H^2
$$

$$
\lesssim \log T \varepsilon_s^2 + \frac{\log^2 T}{T} \varepsilon_H^2. \tag{66}
$$

This completes the proof.

C EXPERIMENT DETAILS

C.1 EXPERIMENT SETTING

Synthetic 1D and 2D mixture experiments. We conducted experiments on synthetic 1D and 2D mixture distributions to evaluate the performance of our Likelihood Matching (LM) and Score Matching (SM) methods under controlled conditions. In the non-oracle setting, where the true parametric form of the data distribution is unknown, we trained fully connected neural networks with a single hidden layer and ReLU activation functions to approximate the score and covariance terms. Models were trained for 500 epochs using the Adam optimizer with a learning rate of 0.01 and full-batch gradient descent.

Real image datasets. We further evaluated our method on several standard image generation benchmarks: MNIST (32×32 grayscale, Deng 2012), CIFAR-10 (32×32 RGB), CelebA (64×64 RGB, Liu et al. 2015), LSUN Church and LSUN Bedroom (64×64 RGB, Yu et al. 2016). All image data were normalized to the range $[-1, 1]$.

We adopted a U-Net architecture for both the score function and the Hessian function approximation, following previous work in score-based diffusion modeling. For the Hessian network, the number of output channels is set to $(r+1) \times C$, where r is the predefined low-rank parameter and C denotes the number of image channels. The Hessian function is modeled using a spiked structure following Meng et al. (2021):

$$
H_t(X_t; \phi) = \boldsymbol{U}_t(X_t; \phi) + \boldsymbol{V}_t(X_t; \phi)\boldsymbol{V}_t(X_t; \phi)^T,
$$

where $\boldsymbol{U}_t \in \mathbb{R}^d$ is a diagonal matrix and $\boldsymbol{V}_t \in \mathbb{R}^{d \times r}$ represents the low-rank component. We applied a ReLU activation to the output of $\boldsymbol{U}_t$ to ensure the positive definiteness of H_t.

In the experiments, we set time steps $T = 1$. For clarity, the score network uses a standard U-Net with 4 down/up blocks, 2 ResNet layers per block, and channels (128, 256, 256, 512), with attention in the third down and second up blocks. The Hessian network follows the same structure but uses 1 ResNet layer per block and smaller channels (64, 128, 128, 128). Its output is $(1 + r)$ times the input channels, representing a diagonal-plus-low-rank structure following Meng et al. (2021).

All models were trained for 500,000 iterations using the Adam optimizer with $(\beta_1, \beta_2) = (0.9, 0.999)$ and a learning rate of 10^{-4}. We adopted a linear noise schedule with $\beta(0) = 0.1$ and $\beta(T) = 20$, consistent with the settings in Song et al. (2021c). Training was performed on NVIDIA A100 GPUs. The batch size was set to 128 for MNIST and CIFAR-10, and 64 for CelebA, LSUN Church, and LSUN Bedroom. We applied Exponential Moving Average (EMA) to model parameters with a decay rate of 0.9999 to improve stability during training and sampling. For evaluation, we computed the Fréchet Inception Distance (FID) using the `torchmetrics` module with feature dimension 2048. FID was calculated based on 10,000 generated samples per dataset. Prior to evaluation, all images were resized and center-cropped to 299×299 pixels, and grayscale images (e.g., MNIST) were replicated across the RGB channels to match the input format of the InceptionV3 model. For likelihood evaluation, we compute the NLL directly under the discrete SDE by evaluating the exact Gaussian likelihood of the residuals using the learned covariance.

C.2 Additional results

Figure 3 shows us the comparisons between the discrepancies between the original data (Mixture Gaussian) and the synthetic data by LM. In particular, for the one-dimensional case, we use the kernel density estimation tool to visualize the densities obtained from both synthetic data and the original data in Figure 3a. For the two-dimensional case, we illustrate the difference between the synthetic data and the original data using scatter plots in Figure 3b. From both figures, we see that our synthetic data indeed learn the associated underlying densities of the original data.

Figure 5 also presents sample generations from the Likelihood Matching method ($N = 2$, $r = 10$) on the CIFAR10, CelebA, LSUN Church and LSUN Bedroom datasets.

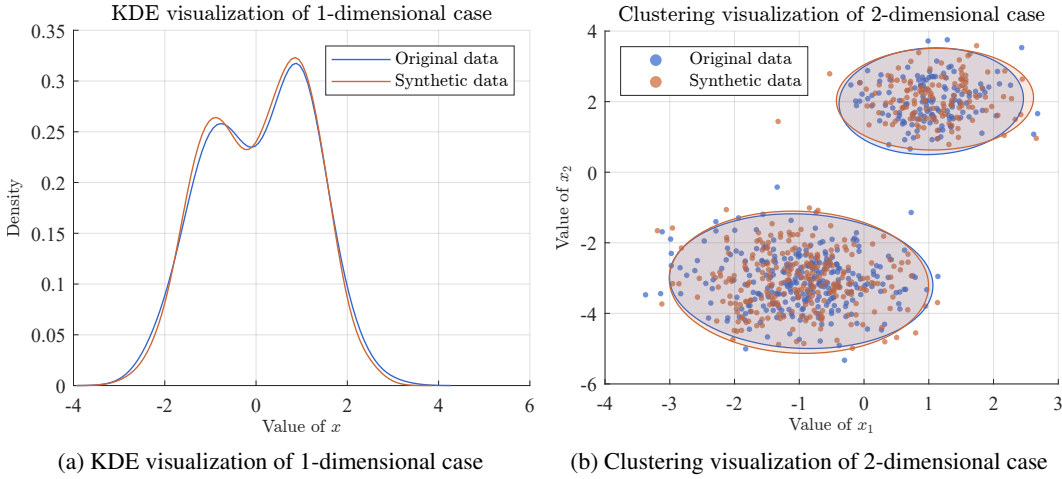(a) KDE visualization of 1-dimensional case   (b) Clustering visualization of 2-dimensional case

Figure 3: Comparison of original and synthetic data. (a) Kernel Density Estimations (KDE) for the 1-dimensional case. (b) Clustering results for the 2-dimensional case.

C.3 Computational Analysis

While introducing a Hessian network increases computational overhead, our framework remains scalable due to the low-rank approximation and efficient implementation using the Sherman-Morrison-Woodbury formula (see Appendix C.4). On a single A100 GPU for CIFAR-10, training time per iteration increased from 0.291s (SM) to a manageable 0.599s for a diagonal Hessian ($r = 0$) and 0.756s for $r = 200$. Similarly, sampling time per 1000 steps grew from 12.66s to 27.65s. This analysis demonstrates a favorable trade-off between performance gains and computational cost. A detailed breakdown of runtime and memory usage is available in Table 3.

Memory usage also scaled controllably with Hessian rank r, remaining well within the practical limits. Specifically, the full training required 36.2GB to 40.4GB ($r = 0$ to 200), representing 1.7-2.1 times of the SM baseline (17.2GB). Crucially, our Hessian-only training mode, where the score network remained fixed, reduced the overhead to just 8.3GB ($r = 0$) to 13.3GB ($r = 200$). Growing
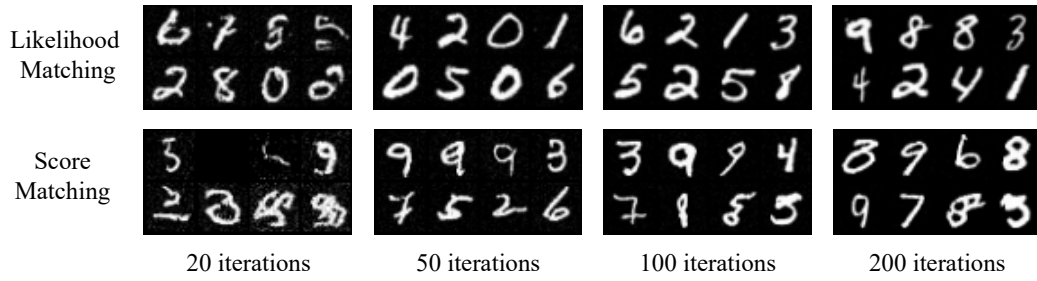
Figure 4: Sampling on MNIST. Both Likelihood Matching and Score Matching use the sampler (13), with the Hessian function set to zero in the case of Score Matching.

Figure 5: Unconditional samples generated by proposed method on 32×32 CIFAR10 (top two rows), 64×64 CelebA (upper middle), 64×64 LSUN Church (lower middle), and 64×64 LSUN Bedroom (bottom row).

Table 2: Comparison of parameter estimations for the two-dimensional mixture

(a) Estimation by Likelihood Matching

Parameter	$n = 100$		$n = 200$	
	MAE	Std. Error	MAE	Std. Error
μ_{11}	**0.0840**	**0.1065**	**0.0596**	**0.0733**
μ_{12}	**0.0838**	**0.1045**	**0.0549**	**0.0698**
μ_{21}	**0.0842**	**0.1057**	**0.0591**	**0.0727**
μ_{22}	**0.0841**	**0.1039**	**0.0627**	**0.0783**
σ_1	0.2550	**0.0556**	0.2520	**0.0364**
σ_2	0.1831	**0.0753**	0.1814	**0.0531**
ω_1	**0.1249**	**0.1529**	**0.0829**	**0.1042**

(b) Estimation by Score Matching

Parameter	$n = 100$		$n = 200$	
	MAE	Std. Error	MAE	Std. Error
μ_{11}	0.1137	0.1408	0.0800	0.0985
μ_{12}	0.1092	0.1344	0.0768	0.0955
μ_{21}	0.1185	0.1500	0.0853	0.1079
μ_{22}	0.1164	0.1480	0.0840	0.1064
σ_1	**0.2519**	0.0745	**0.2468**	0.0508
σ_2	**0.1818**	0.0990	**0.1820**	0.0707
ω_1	0.1566	0.1923	0.1154	0.1409

r from 100 to 200 increased memory by only 16% (11.5GB to 13.3GB), demonstrating efficient memory management even at high approximation fidelity.

The computing comparison results on high-resolution ImageNet are shown in Table 4, which indicate that the computational burden increases notably at higher resolution and may require further, dedicated research to fully address.

Table 3: Training and sampling cost of the LM with different Hessian ranks r on CIFAR-10 (A100, batch size 256). "Hessian Time" and "Hessian Mem" refer to the additional cost of training the Hessian alone with a fixed score network.

	Training Time (s/it)	Training Mem (MB)	Hessian Time (s/it)	Hessian Mem (MB)	Sampling Time (s/1000 iters)
SM	0.291	17,247	/	/	12.66
LM ($r = 0$)	0.599	36,220	0.303	8,286	20.83
LM ($r = 20$)	0.617	36,428	0.324	8,418	21.48
LM ($r = 100$)	0.664	38,822	0.369	11,452	23.61
LM ($r = 200$)	0.756	40,444	0.463	13,302	27.65

Table 4: Training and sampling cost of the LM with different Hessian ranks r on 224×224 ImageNet (A100, batch size 4). "Hessian Time" and "Hessian Mem" refer to the additional cost of training the Hessian alone with a fixed score network.

	Training Time (s/it)	Training Mem (MB)	Hessian Time (s/it)	Hessian Mem (MB)	Sampling Time (s/1000 iters)
SM	0.155	17,183	/	/	34.6
LM ($r = 0$)	0.566	49,287	0.362	28,943	68.5
LM ($r = 20$)	0.571	49,641	0.370	29,057	69.8
LM ($r = 100$)	0.583	50,213	0.384	29,913	71.2
LM ($r = 200$)	0.598	51,357	0.403	31,163	74.0

C.4 EFFICIENT IMPLEMENTATION OF TRAINING AND SAMPLING PROCEDURE

Likelihood Matching training and inference involve repeated evaluations of computationally intensive linear algebra operations, including matrix inversion, matrix square roots, and determinant calculations. Given that image data typically resides in high-dimensional spaces (e.g., $d > 1000$), the associated computational cost, on the order of $\mathcal{O}(d^3)$, becomes prohibitive in practice. To mitigate this issue, we adopt the diagonal-plus-low-rank covariance parameterization proposed by Meng et al. (2021), modeling the covariance as

$$H_t(X_t; \phi) = \boldsymbol{U}_t(X_t; \phi) + \boldsymbol{V}_t(X_t; \phi)\boldsymbol{V}_t(X_t; \phi)^T,$$

where $\boldsymbol{U}_t(\cdot; \phi) : \mathbb{R}^d \to \mathbb{R}^{d \times d}$ is a diagonal matrix, and $\boldsymbol{V}_t(\cdot; \phi) : \mathbb{R}^d \to \mathbb{R}^{d \times r}$ is a low-rank matrix with a prespecified rank $r \ll d$. For notational simplicity, we omit the dependence on $(X_t; \phi)$ and associated superscripts/subscripts.

This structural assumption enables a series of simplifications that substantially reduce the computational cost of matrix operations.

Lemma 6. *For any vector $X \in \mathbb{R}^d$, we have the following equalities:*

$$\left| I_d + \sigma^2 \boldsymbol{U} + \sigma^2 \boldsymbol{V}\boldsymbol{V}^T \right| = \left| I_d + \sigma^2 \boldsymbol{U} \right| \cdot \left| I_r + \tilde{\boldsymbol{V}}^T \tilde{\boldsymbol{V}} \right|, \tag{67}$$

$$X^T \left(I_d + \sigma^2 \boldsymbol{U} + \sigma^2 \boldsymbol{V}\boldsymbol{V}^T \right)^{-1} X = \tilde{X}^T \tilde{X} - (\tilde{\boldsymbol{V}}^T \tilde{X})^T (I_r + \tilde{\boldsymbol{V}}^T \tilde{\boldsymbol{V}})^{-1} (\tilde{\boldsymbol{V}}^T \tilde{X}), \tag{68}$$

$$\left(I_d + \sigma^2 \boldsymbol{U} + \sigma^2 \boldsymbol{V}\boldsymbol{V}^T \right)^{1/2} X = (I_d + \sigma^2 \boldsymbol{U})^{1/2}(X + \tilde{\boldsymbol{V}}\boldsymbol{\Gamma}\{(\boldsymbol{\Lambda} - I_r)^{1/2} - I_r\}\boldsymbol{\Lambda}^{-1}\boldsymbol{\Gamma}^T \tilde{\boldsymbol{V}}^T X), \tag{69}$$

where $\tilde{X} = (I_d + \sigma^2 \boldsymbol{U})^{-1/2}X$, $\tilde{\boldsymbol{V}} = \sigma(I_d + \sigma^2 \boldsymbol{U})^{-1/2}\boldsymbol{V}$ and $\boldsymbol{\Gamma}^T \boldsymbol{\Lambda}\boldsymbol{\Gamma} = \tilde{\boldsymbol{V}}^T \tilde{\boldsymbol{V}}$ is the eigendecomposition.

Proof. Equation (67) can be directly obtained by the matrix determinant lemma. For (68), denote $\boldsymbol{B} = I_d + \sigma^2 \boldsymbol{U}$. Applying the Sherman-Morrison-Woodbury formula yields:

$$X^T \left(I_d + \sigma^2 \boldsymbol{U} + \sigma^2 \boldsymbol{V}\boldsymbol{V}^T \right)^{-1} X = X^T \boldsymbol{B}^{-1}X - X^T \sigma^2 \boldsymbol{B}^{-1}\boldsymbol{V}(I_r + \boldsymbol{V}^T\boldsymbol{B}^{-1}\boldsymbol{V})\boldsymbol{V}^T\boldsymbol{B}^{-1}X,$$

followed by (68) via defining $\tilde{X} = (I_d + \sigma^2 \boldsymbol{U})^{-1/2}X$ and $\tilde{\boldsymbol{V}} = \sigma(I_d + \sigma^2 \boldsymbol{U})^{-1/2}\boldsymbol{V}$. bUpsilon For (69), since $\left(\boldsymbol{B} + \sigma^2 \boldsymbol{V}\boldsymbol{V}^T \right)^{1/2} X = \boldsymbol{B}^{1/2}(I_d + \tilde{\boldsymbol{V}}\tilde{\boldsymbol{V}}^T)^{1/2}\tilde{X}$. Consider SVD such that $\tilde{\boldsymbol{V}} = \boldsymbol{\Upsilon}\boldsymbol{\Lambda}^{1/2}\boldsymbol{\Gamma}^T$, where $\boldsymbol{\Upsilon} \in \mathbb{R}^{p \times r}$ with orthogonal columns, $\boldsymbol{\Gamma} \in \mathbb{R}^{r \times r}$ is orthogonal and $\boldsymbol{\Lambda} \in \mathbb{R}^{r \times r}$ is a diagonal matrix. Then since $I_d + \tilde{\boldsymbol{V}}\tilde{\boldsymbol{V}}^T = \boldsymbol{\Upsilon}(I_d + \boldsymbol{\Lambda})\boldsymbol{\Upsilon}^T + (I_p - \boldsymbol{\Upsilon}\boldsymbol{\Upsilon}^T)$, therefore

$$(I_d + \tilde{\boldsymbol{V}}\tilde{\boldsymbol{V}}^T)^{1/2} = I_d - \boldsymbol{\Upsilon}[I_r - (I_r + \boldsymbol{\Lambda})^{-1/2}]\boldsymbol{\Upsilon}^T.$$

Because $\boldsymbol{\Upsilon} = \tilde{\boldsymbol{V}}\boldsymbol{\Lambda}^{-1/2}\boldsymbol{\Gamma}^T$, substitute it into the former equation and notice that $\tilde{\boldsymbol{V}}^T \tilde{\boldsymbol{V}} = \boldsymbol{\Gamma}\boldsymbol{\Lambda}\boldsymbol{\Gamma}^T$, we have

$$(I_d + \tilde{\boldsymbol{V}}\tilde{\boldsymbol{V}}^T)^{1/2} = I_d - \tilde{\boldsymbol{V}}[(I_r + \tilde{\boldsymbol{V}}^T \tilde{\boldsymbol{V}})^{1/2} - I_r](\tilde{\boldsymbol{V}}^T \tilde{\boldsymbol{V}})^{-1}\tilde{\boldsymbol{V}}^T,$$

Finally, by eigen-decompositions, we have

$$\left(I_d + \sigma^2 \boldsymbol{U} + \sigma^2 \boldsymbol{V}\boldsymbol{V}^T \right)^{1/2} X = (I_d + \sigma^2 \boldsymbol{U})^{1/2}(X + \tilde{\boldsymbol{V}}\boldsymbol{\Gamma}\{(\boldsymbol{\Lambda} - I_r)^{1/2} - I_r\}\boldsymbol{\Lambda}^{-1}\boldsymbol{\Gamma}^T \tilde{\boldsymbol{V}}^T X).$$

$\square$